ISAS - INTERNATIONAL SCHOOL FOR ADVANCED STUDIES

HYDROGEN IN SILICON: A FIRST PRINCIPLES MOLECULAR DYNAMICS STUDY

Thesis submitted for the degree of
"Doctor Philosophiæ"

CANDIDATE
Francesco Buda

SUPERVISORS
Prof. Roberto Car
Prof. Michele Parrinello

December 1989

TRIESTE

SISSA - SCUOLA INTERNAZIONALE SUPERIORE DI STUDI AVANZATI
TRIESTE
Strada Costiera 11

International School for Advanced Studies
Trieste

HYDROGEN IN SILICON: A FIRST PRINCIPLES MOLECULAR DYNAMICS STUDY

Thesis submitted for the degree of
"Doctor Philosophiæ"

CANDIDATE
Francesco Buda

SUPERVISORS
Prof. Roberto Car
Prof. Michele Parrinello

December 1989

Contents

Introduction

The role played by hydrogen (H) when incorporated into semiconducting materials, has recently attracted a vast interest. This stems from the fact that the presence of H causes important changes in the electrical and optical properties of semiconductors, both in their crystalline and amorphous phases. A clear understanding of these phenomena is of great technological relevance.

In crystalline semiconductors an important phenomenon is the ability of H of passivating the electrical activity of shallow acceptor and donor impurities [1]. Because shallow levels determine the doping of the semiconductor, and therefore its characteristics in electronic devices, it is essential to be able to understand and then to control the effects of the presence of hydrogen.

In amorphous silicon (a-Si), the key role played by hydrogen is the saturation of dangling bonds. Indeed, pure a-Si contains many dangling bonds that give rise to a large density of localized states within its energy gap. Hydrogen saturates these dangling bonds and therefore sensibly reduces the density of gap states. This confers semiconducting properties to the material, which makes it possible to dope it. This property has increased enormously the interest in hydrogenated amorphous silicon (a-Si:H) and allowed for a technological application of this material to fabricate thin-film electronic devices, including solar cells [2].

It is only recently that theoretical efforts have been devoted to the

understanding of hydrogen behaviour in semiconductors. Indeed, only in recent years, theoretical instruments have become available, which allow for reliable investigations of these complex materials. In particular, ab-initio total energy calculations within Density Functional Theory (DFT) [3,4] have proven to be very accurate and successful for the study of different properties of semiconducting systems [5]. Recently, total energy calculations have allowed to describe the energy surface for H both in pure and doped crystalline silicon (c-Si) for different charge states [6].

However, this theoretical approach suffers two basic limitations: (i) it is restricted to the study of static (zero temperature) properties; (ii) the structure of the system to examine must be an input of the problem.

The latter is a strong limitation expecially when studying disordered systems, as in the case of amorphous semiconductors.

Few years ago Car and Parrinello [7] extended the applicability of the DFT approach to a larger variety of condensed matter systems. They proposed a method that combines the DFT formalism with Molecular Dynamics simulations. This scheme allows to describe the dynamics of the ions (treated as classical particles), under the action of forces generated directly from the ground state electronic energy, according to the Born-Oppenheimer approximation. Therefore within this approach, structural and dynamical properties at finite temperature become accessible to first principles calculations. Furthermore, it is possible to generate via thermal treatment disordered systems, and to study details of their local order that are in general inaccessible to experiments.

In this thesis we focus our attention on silicon and on the effects of hydrogen incorporation both in its crystalline and amorphous phases. The outline is the following:

In the first chapter we discuss the basic ideas of the theoretical approach for ab-initio molecular dynamics, and illustrate how it works.

Chapter 2 discuss the properties of pure c-Si at finite temperature: it is shown that thermodynamic properties can be calculated with an accuracy comparable with that usually obtained for equilibrium structural properties.

In Chapter 3 we present a study of the diffusive behaviour of an isolated positively charged H in c-Si. This is a phenomenon of basic relevance to the interpretation of the effects of H in silicon. We analyze microscopic details of this process that are inaccessible to experiments, and furthermore we can make a direct comparison with experimental findings. Our results demonstrate the importance of dynamical effects that previous theoretical works were not able to deal with.

In the last chapter the results of a recent simulation on an a-Si:H sample numerically generated, are discussed. In particular, we analyze the short range order and the vibrational properties of this material. The comparison with existing experiments shows a very good agreement. Some insight on the diffusion of H in this material is provided by observed relaxation phenomena. A possible explanation of a clustering effect of H in a-Si:H, which is also observed experimentally, is given.

Chapter 1

The Car-Parrinello method

1.1 Introduction

A unified approach to Molecular Dynamics (MD) and Density Functional Theory (DFT) has been proposed a few years ago by Car and Parrinello [7]. In this chapter, we briefly recall and discuss the main ideas of this approach, which will be referred to, in the following, as the MD-DF method.

Molecular Dynamics simulations are a powerful numerical tool for the study of equilibrium and non-equilibrium properties of complex condensed matter systems [8]. Within this scheme, the classical equations of motion for the atoms are explicitly solved and equilibrium statistical averages can be computed as temporal averages over the MD observation time, according to the ergodic hypothesis. The MD approach can represent a bridge between theory and experiment and allows for the investigation of microscopic details of the atomic motion that are generally inaccessible to measurements. Since MD simulations usually treat the atomic motion as classical, the conclusions that can be drawn from this analysis are valid if quantum effects on the atomic motion can be neglected, and if the Born-Oppenheimer (BO) approximation holds. In other words, it is implicitly assumed that the electrons are always in the

ground-state corresponding to the instantaneous nuclear configuration. These conditions are satisfied in most cases of interest.

The main problem connected with MD simulations is the choice of an appropriate interatomic potential. Empirical potentials, containing two-body terms, have been largely used for simulating simple systems like rare gases. If these potentials can be useful for systems where the electronic charge density is almost rigid around the atom, they become unreliable when applied to systems where the distribution of the charge density changes significantly in response to the atomic motion, as is the case for semiconductors. Effective potentials for tetrahedral semiconductors containing 2- and 3-body terms [9,10,11] have been recently constructed, whose parameters are fitted to experimental data. Although partially successful in reproducing some properties of these systems, they suffer some basic limitations: (i) it is difficult to assess the transferability of the potential to thermodynamic states different from that used for its generation; (ii) this approach completely misses the important correlation existing between local electronic structure and atomic dynamics.

The basic idea of the MD simulation scheme proposed by Car and Parrinello is to obtain the interatomic potential directly from the adiabatic (Born-Oppenheimer) electronic ground state, corresponding to the instantaneous ionic configuration. Situations in which the electrons do not follow adiabatically the ionic motion (non BO dynamics), cannot be accounted for within this scheme: in this case one should treat both ions and electrons with quantum mechanics.

In the MD-DF scheme, the electronic ground state is treated within the DFT [3,4]: in such approach the complex many body problem is converted into the solution of a set of self-consistent single-particle equations. These equations have been most commonly solved by using the

Local Density Approximation (LDA) for the exchange and correlation energy [4,12]. In the MD-DF scheme, the single particle electronic orbitals (expanded on a basis set) are treated as classical degrees of freedom on the same footing as the ionic coordinates. The fictitious dynamics that governs the motion of electrons is such that the electrons are at any time very close to the ground state relative to the instantaneous ionic configuration. In this way the ions move on the BO potential surface and finite temperature ionic properties can be computed. Moreover, MD-DF simulations allow at the same time for the calculation of the variation of the electronic properties due to the ionic motion.

1.2 Minimization of the energy functional: the Born-Oppenheimer surface

Within DFT, the problem of computing the total energy ground-state of a system of interacting electrons and nuclei corresponds to the search for the minimum of a unique functional $E[n(\mathbf{r}), \{\mathbf{R}_I\}]$ of the electronic density n($\mathbf{r}$), for every fixed nuclear configuration $\{\mathbf{R}_I\}$. Following the idea of Kohn and Sham [4] (KS), the electronic density n($\mathbf{r}$) can be expressed in terms of occupied single-particle orbitals:

$$n(\mathbf{r}) = \sum_i f_i \mid \psi_i(\mathbf{r}) \mid^2 \tag{1.1}$$

where f_i is the occupation number of the orbital ψ_i. Therefore, in principle, the BO potential energy surface for the nuclei $\Phi(\{\mathbf{R}_I\})$, can be obtained by minimizing the functional $E[\{\psi_i\}, \{\mathbf{R}_I\}]$ with respect to the electronic degrees of freedom $\{\psi_i\}$:

$$\Phi(\{\mathbf{R}_I\}) = min_{\{\psi_i\}} E[\{\psi_i\}, \{\mathbf{R}_I\}] \tag{1.2}$$

The explicit expression of the functional E is:

$$E[\{\psi_i\},\{\mathbf{R}_I\}] = \sum_i f_i \int d\mathbf{r}\psi_i^*(\mathbf{r})[-\frac{1}{2}\nabla^2]\psi_i(\mathbf{r}) + \int d\mathbf{r}V^{ext}(\mathbf{r})n(\mathbf{r}) + \frac{1}{2}\int d\mathbf{r}d\mathbf{r}'\frac{n(\mathbf{r})n(\mathbf{r}')}{\mid \mathbf{r}-\mathbf{r}' \mid} + E^{xc}[n] + \frac{1}{2}\sum_{I\neq J}\frac{Z_I Z_J}{\mid \mathbf{R}_I - \mathbf{R}_J \mid} \qquad (1.3)$$

where atomic units have been adopted. V^{ext} is the electrostatic potential of the nuclei felt by the electrons, Z_I is the nuclear charge and $E^{xc}[n]$ is the interaction energy between electrons beyond the Hartree term, that is the exchange and correlation energy, which is expressed as a functional of the charge density n(r). In practice, in most DFT calculations, and in particular in the MD-DF scheme, this functional is written within the LDA, i.e. the exchange and correlation potential at the point r is assumed to depend only on the charge density at the same point. This approximation has been proven to be very reliable for the prediction of many properties, such as the equilibrium lattice structure, phonon frequencies and elastic constants [13], of a variety of systems.

A further simplification often used in DFT calculations is the introduction of pseudopotentials. The core electrons are assumed to be frozen in their atomic configuration and not to take part in the chemical bonding. The nucleus plus the core electrons are then replaced by a "pseudoion" of charge Z_V, corresponding to the valence charge; the interaction between the valence electrons and this pseudoion is described by an appropriate effective potential. Within a pseudopotential scheme, in Eq. (1.3) the external potential V^{ext} is substituted by a sum of ionic pseudopotentials and the nuclear charge by Z_V. State-of-the-art electronic calculations adopt generally nonlocal, norm-conserving pseudopotentials, generated from all-electron first principles atomic calculations [14,15]. Such pseudopotentials have been shown to have good

transferability properties from one chemical environment to another, for many systems of interest.

The minimization problem stated by Eq. (1.2), with the constraint that the wavefunctions be orthonormal:

$$\int d\mathbf{r}\psi_i^*(\mathbf{r})\psi_j(\mathbf{r}) = \delta_{ij} \tag{1.4}$$

has generally been faced by solving the associated Kohn-Sham [4] equations:

$$[-\frac{1}{2}\nabla^2 + V]\psi_i(\mathbf{r}) = \varepsilon_i\psi_i(\mathbf{r}) \tag{1.5}$$

where V is the sum of three terms: the external potential $V^{ext}(\mathbf{r})$, the Hartree potential $V^H(\mathbf{r}) = \int d\mathbf{r}' \frac{n(\mathbf{r}')}{|\mathbf{r}-\mathbf{r}'|}$ and the exchange-correlation potential $\mu^{xc}(\mathbf{r}) = \frac{\delta E^{xc}[n]}{\delta n(\mathbf{r})}$. Since V depends on the actual electronic density $n(\mathbf{r})$, equation (1.5) must be solved self-consistently. If the orbitals $\psi_i(\mathbf{r})$ are expanded in terms of a basis set (for instance plane waves), the solution of the Kohn-Sham equations can be converted into a matrix eigenvalue problem, to be solved by iterative diagonalizations. However this approach becomes quickly too demanding computationally, as the size of the system is increased. Furthermore it results particularly inefficient if the geometry of the system is also an unknown of the problem. Indeed, in this case the search for the global minimum of the functional of eq. (1.3) with respect to $\mathbf{R}_I$, requires the whole self-consistent procedure to be repeated several times.

1.2.1 Dynamical simulated annealing

The minimization of the energy functional (1.3) can be thought of as a complex optimization problem, which can be handled with statistical mechanics techniques. In the MD-DF approach, the concept of simulated annealing introduced by Kirkpatrik et al. [16] has been used, but

within an MD strategy rather than within a Monte Carlo (MC) procedure, as first proposed in ref. [16].

Within this scheme, it is possible to obtain simultaneously the self-consistent electronic ground state and the global minimum of the energy functional E. Both the ionic and the electronic degrees of freedom are considered as classical time dependent variables. An appropriate Lagrangian is introduced for the coupled electronic and ionic system, in which the potential is just the energy functional which needs to be minimized. From this Lagrangian, a classical dynamics is generated, according to which the system, at a given temperature, explores the associated configuration space determined by its total energy. If then the system is slowly cooled down by subtracting kinetic energy, the regions of configuration space that can sampled are gradually reduced and, when the temperature goes to zero, the point of minimum potential is eventually recovered.

The simulated annealing scheme for computing the minimum of the Energy functional is necessary when the hyper-space of the degrees of freedom of the problem is particularly complicated, and various local minima in which the system can be trapped are present. This is the case, for example, in the search of equilibrium geometries for microclusters: the dynamical simulated annealing method has indeed been successfully used for a variety of small clusters [17,18,19,20,21,22].

However, when the potential energy of the system does not present local minima, the annealing process appears to be unnecessary. Experience has shown that, if the ionic positions are kept fixed (i.e. in the case of simple electronic optimization), only a single minimum is encountered in LDA calculations. Therefore in this case, the use of a simulated annealing technique is inefficient, since the convergence to the minimum would be rather slow. More efficient dynamical techniques can

be adopted, like steepest descent (SD) or conjugate gradient (CG). We will not enter into the details of these procedures here, but refer to the work of ref. [23], where an accurate analysis and a comparison of the various algorithms is presented. We want now to discuss the idea of using the dynamics not just as an alternative way of finding the ground-state total energy of a system, but for simulating real BO trajectories for the nuclei.

1.3 Ab-initio Molecular Dynamics

The MD-DF method is based on the introduction of a fictitious classical dynamics for the coupled evolution of the ions and the KS orbitals. The dynamics is generated by the classical Lagrangian:

$$L = \sum_i \mu \int_\Omega d\mathbf{r} |\dot{\psi}_i|^2 + \sum_I \frac{1}{2} M_I \dot{\mathbf{R}}_\mathbf{I}^2 - E[\{\psi_i\}, \{\mathbf{R}_I\}] + \sum_{ij} \Lambda_{ij} \left(\int_\Omega d\mathbf{r} \psi_i^*(\mathbf{r}) \psi_j(\mathbf{r}) - \delta_{ij} \right) \tag{1.6}$$

where M_I are the ionic masses, μ is a fictitious mass associated to the time dependent KS orbitals $\psi_i(\mathbf{r}, t)$, that controls the time scale of the electronic motion; the dots indicate time derivatives; Λ_{ij} are Lagrangian multipliers used to impose the orthonormality constraints on the ψ_i, Ω is the volume of the system and $E[\{\psi_i\}, \{\mathbf{R}_I\}]$ is the energy functional defined in eq. (1.3). The classical equations of motion derived from the Lagrangian (1.6) are:

$$\mu \ddot{\psi}_i = -\frac{\delta E}{\delta \psi_i^*(\mathbf{r}, t)} + \sum_j \Lambda_{ij} \psi_j(\mathbf{r}, t) \tag{1.7}$$

$$M_I \ddot{\mathbf{R}}_I = -\frac{\partial E}{\partial \mathbf{R}_I(t)} \tag{1.8}$$

The second term on the right of eq. (1.7) represents the constraint force acting on the ψ_i. Eq. (1.7) has a form analogous to that of the equations of conventional MD for molecules, in which the separation between the atoms is kept fixed during the dynamics. The constraints expressed by Eq. (1.4) can be interpreted as rigidity constraints: They are time-independent, holonomic constraints and they do not lead to any energy dissipation. The way for treating such constraints has been studied within conventional MD by Ryckaert et al. [24]. These authors have developed an algorithm which allows the constraints to be satisfied at each time step during the simulation, and the system to be conservative.

The question is how the above equations of motion can be useful to generate physical trajectories for the ions. Suppose we have performed a dynamical simulated annealing, or whatever else dynamical procedure for reaching the minimum of the energy functional (1.3). In any case, at the end of the minimization all the velocities $\dot{\psi}_i$ are zero, and therefore the kinetic term associated to the electronic degrees of freedom, $K_e = \sum_i \mu \int_\Omega d\mathbf{r} |\dot{\psi}_i|^2$, is also zero. Furthermore the functional $E[\{\psi_i\}, \{\mathbf{R}_I\}]$ coincides with the BO potential $\Phi(\{\mathbf{R}_I\})$ (here $\{\mathbf{R}_I\}$ does not necessarily coincide with the equilibrium configuration for the system). We note that, during the minimization procedure, the value of the masses M_I and μ used in the equations of motion can be chosen freely in such a way as to optimize the convergence of the algorithm to the minimum.

Once the previous conditions have been reached, the real dynamics for the ions on the BO potential surface can be started. To this end, a "metastable" situation is devised, in which the electronic degrees of freedom follow adiabatically the ionic motion, without significantly acquiring kinetic energy (K_e). K_e is in some sense a measure of how much the ψ's deviate from the BO surface, during the dynamics. The mass M_I

appearing in Eq. (1.8) is now the physical ionic mass, and the choice of μ becomes relevant in order to make the ionic and electronic subsystems decoupled. In practice, the ratio $\frac{\mu}{M_I}$ should be much less than 1; in such a way the characteristic frequencies of the fictitious electronic dynamics are very high with respect to those associated with the ionic motion, making the two subsystems decoupled. A numerical consequence of this choice for the parameter μ is that the time step Δt used in the numerical integration of the equations of motion must be smaller (typically $\Delta t \simeq 10^{-16} sec$) than, e.g., the time steps adopted in conventional MD simulations.

We call the metastable situation in which the electronic degrees of freedom do not thermally equilibrate with the ionic ones, a classical adiabatic dynamics. In fact, if the system evolves dynamically for a very long time, eventually thermal equilibrium will be reached. In practice, the rate at which this equilibration takes place is required to be slow with respect to the typical observation time of an MD run. In such a way, one can evaluate temporal averages for quantities of interest, along trajectories that lie very close to the BO surface.

Experience has shown that, for both crystalline [25] and disordered systems [26,27], this classical adiabatic dynamics is very well accomplished for insulators and semiconductors: The kinetic energy K_e has been found to stay very small, and on average constant, over entire MD runs (typically for times of the order of 1 psec or more), to indicate that no transfer of energy between ionic and electronic degrees of freedom was occurring. Furthermore, this behaviour does not seem to depend strongly on the temperature of the ionic system.

1.3.1 An illustrative application to c-Si

To illustrate more in detail the way in which the adiabatic dynamics works, we have considered a system consisting of 16 silicon atoms in an FCC box with periodic boundary conditions. The silicon atoms are placed initially in the perfect crystalline configuration. The single particle electronic orbitals are expanded in plane waves up to a cut-off in energy of 6 Ry. The Brillouin zone has been sampled with the Γ point. The equations of motions (1.7) and (1.8) have been numerically solved by using the Verlet algorithm [28] (see Appendix B.) with a time step $\Delta t = 7a.u.$. We set the mass parameter $\mu = 300a.u.$. The ionic subsystem has been heated up to $\simeq 400K$ by simply rescaling the velocities and then the system has been allowed to evolve freely under the action of the Lagrangian (1.6). The dynamics starts with the electronic degrees of freedom at the ground state relative to the initial ionic configuration. The algorithm of ref. [24] has been used for the orthonormalization procedure. In fig. 1.1(upper) we plot the ionic kinetic energy $K_I = \sum_I \frac{1}{2} M_I \dot{\mathbf{R}}_\mathbf{I}^2$, $E\left[\{\psi_i\}, \{\mathbf{R}_I\}\right]$ and their sum U_I'. On the scale of the picture $U_I' \approx$ constant. However if we enlarge the scale by two orders of magnitude as in fig. 1.1(lower), U_I' shows some variations. These are exactly compensated by the electronic kinetic term K_e, also shown in the picture, leading to constant $U_{eI} = U_I' + K_e$ within numerical accuracy. This demonstrates clearly that, as expected, the dynamics generated by the Lagrangian (1.6) conserves the total internal energy U_{eI}. The variations in U_I' are much smaller than the typical variations in either K_I or $E\left[\{\psi_i\}, \{R_I\}\right]$. No canonical drift in U_I' is observed. This corresponds to a metastable situation in which the temperature of the electrons is much smaller than that of the ions. The life-time of this metastable state is much longer than typical ionic relaxation times. Indeed we have continued the run for a time of about 1.5 *psec* and we have not ob-

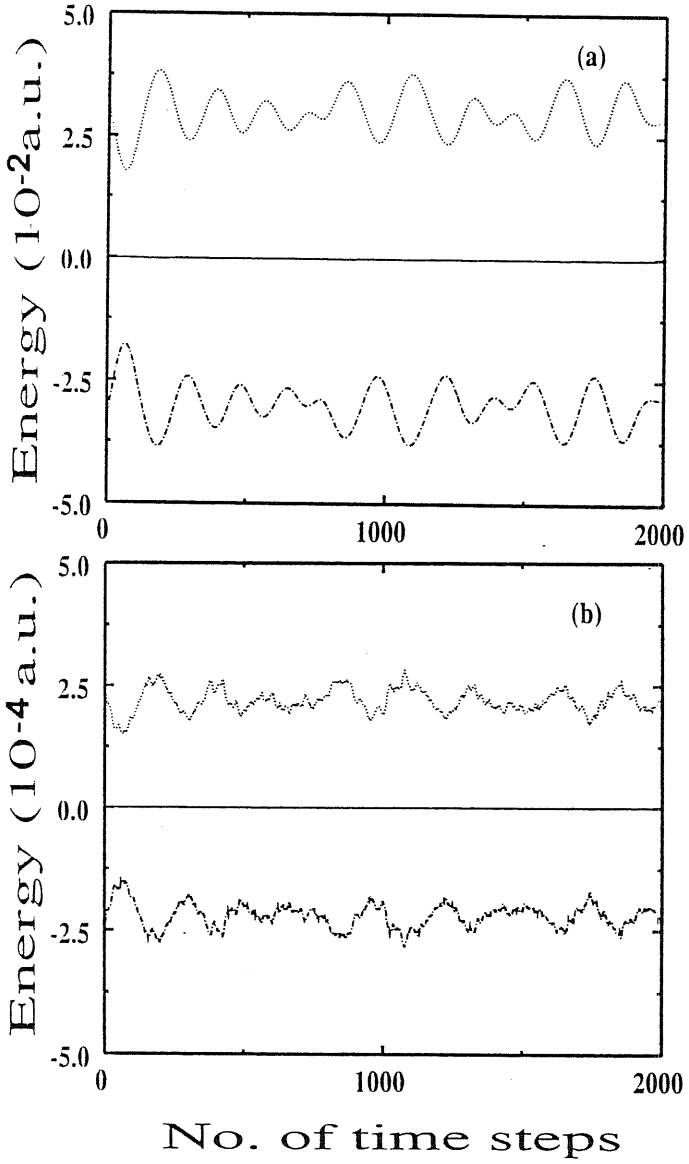

Figure 1.1:
Time variation of electronic and ionic properties for a segment of 2000 time steps of a much larger run (Δt = 7 a.u., μ = 300 a.u.). (upper part) K_I (dotted line), $E\left[\{\psi_i\},\{R_I\}\right]$ (dash-dotted line), U_I' (full line); (lower part) K_e (dotted line), U_I' (dash-dotted line), U_{eI} (full line). E, U_I', U_{eI} are measured relative to the initial value $U_{eI} = -61.62887$ a.u.

served any appreciable drift in U_I'. As a consequence of this adiabatic behaviour K_e in our run remained very small with no appreciable drift. Since K_e measures the deviation from the Born-Oppenheimer surface, this implies that during the run $E\left[\{\psi_i\},\{\mathbf{R}_I\}\right] \approx \Phi\left(\{R_I\}\right)$. We have numerically checked that this was the case. The smallness of K_e ensures adequate evaluation of the ionic forces.

In order to have adiabatic behaviour it is essential to have overall conservative dynamics. The use of orthonormalization schemes different from the one used here would break energy conservation [29,30]. We performed a dynamical simulation for the same system in which, starting from the same initial conditions, we used the Gram-Schmidt orthonormalization scheme. After the same time as in fig. 1.1, the electronic kinetic energy K_e is equal to $\sim 0.6 a.u.$, the total internal energy U_{eI} is no longer constant and the ionic trajectory rapidly diverges from the correct one. Either alteration of the original scheme led to non Born-Oppenheimer trajectories after a rather short time.

1.3.2 Ab-initio MD for metallic systems

For systems where the density of electronic states at the Fermi energy becomes significantly different from zero, it has been observed that the electronic degrees of freedom progressively acquire kinetic energy. Although the time for equilibration between the two subsystems remains quite long, two unpleasant consequences of this coupling are detected: (i) The forces on the ions become incorrect, and (ii) the ionic system cools down affecting the correct computation of equilibrium properties.

Indeed, the characteristic frequencies of the electronic degrees of freedom appear to relate to the properties of the single particle spectrum of the physical system; in particular they seem to be related to the ratio E_g/μ, where E_g indicates the optical gap [31,32]. For metals, the time

scales of the "electronic" and ionic motion can become comparable and therefore the two subsystems become strongly coupled. Nevertheless, the fictitious dynamics of MD-DF simulations has been proven successful also for metallic systems [33,34], provided periodic minimizations of the electrons to their BO surface are periodically performed. A scheme particularly convenient to compute thermodynamical properties of metals has been found to be the constant temperature-constant volume MD technique, originally proposed by Nosè [35,36] for systems described by classical potentials.

Following the approach proposed in ref. [35,36], a Lagrangian $\mathcal{L}$ for an interacting system of electrons and ions is introduced, with the ions only in thermal equilibrium with an external heat reservoir of fixed temperature T_{ext}:

$$\mathcal{L} = \mathcal{L}_{eI} + \frac{1}{2}Q\left(\frac{\dot{s}}{s}\right)^2 - gK_BT_{ext}ln(s) \tag{1.9}$$

where $\mathcal{L}_{eI}$ is given by Eq. (1.6). s is the degree of freedom associated with the external reservoir in thermodynamic equilibrium with the $\mathcal{N}$ ions of the system; Q is a parameter of dimension (energy)·(time)^2 which plays the role of a *mass* for the motion of s. The second and third terms of the right hand side of Eq. (1.9) are respectively the kinetic and potential energy for the variable s, where g is equal to the number of ionic degrees of freedom $(3 \cdot \mathcal{N})$ and K_B is the Boltzman's constant. Since the ions only are coupled to the external system, the equations of motion for $\{\psi_i\}$ are the same as those derived from the Lagrangian (1.6); the equations of motion for $\{R_I\}$ and s are:

$$M_I\frac{d}{dt}(s\dot{\mathbf{R}}_I) = -s \cdot \nabla_{R_I}E \tag{1.10}$$

$$Q\frac{d}{dt}\left(\frac{\dot{s}}{s}\right) = \sum_I M_I\dot{R}_I^{\,2} - gK_BT_{ext} \tag{1.11}$$

We note that, unlike Eq. (1.8), Eq. (1.10) contains a friction term dependent upon the ionic velocities.

This computational scheme makes it possible to keep the average temperature of the system constant during the MD runs. In addition, the electronic coordinates must be periodically quenched, in order to accomplish a correct computation of time averages. Unlike other constant-temperature MD techniques proposed in the literature, the Nosè approach allows to reproduce the canonical probability density in the phase space of the nuclei.

1.4 Technical details for the implementation

The ideas described so far are quite general and do not depend on the particular basis set we use for the electronic structure description; now we want to be more concrete and we will describe some technical points that are important in the following presentation of the results.

1.4.1 Periodic boundary conditions and basis set

In simulations for bulk systems, the MD box is periodically repeated to infinity, in order to avoid surface effects. This choice is quite natural for a perfect crystal, since the primitive cell containing only few atoms is perfectly replicated in all spatial directions. However even for disordered systems (glasses, liquids), whose Hamiltonian does not have any translational symmetry, periodic boundary conditions (pbc) can still be adopted, provided the MD box is chosen large enough that the imposed periodicity does not affect the dynamics of the system.

Therefore the techniques developed in solid state calculations within DFT, which make explicit use of the translational symmetry of the

hamiltonian, are useful also in the context of MD-DF simulations of both ordered and disordered condensed matter systems.

As a consequence of the periodicity introduced by pbc, the single particle orbitals of eq. 1.1 satisfy the Bloch theorem and can be expanded in planewaves:

$$\psi_{n,\mathbf{k}}(\mathbf{r}) = e^{i\mathbf{k}\cdot\mathbf{r}} \sum_{\mathbf{G}} c^{n,\mathbf{k}}(\mathbf{G}) e^{i\mathbf{G}\cdot\mathbf{r}} \tag{1.12}$$

where $\mathbf{G}$ is a reciprocal lattice vector of the supercell used in the simulation. In the MD-DF scheme, the Fourier components $c^{n,\mathbf{k}}(\mathbf{G})$ of the wavefunctions are treated as time dependent degrees of freedom. The wave vector $\mathbf{k}$ lies within the Brillouin Zone (BZ) of the reciprocal lattice of the supercell. For each $\mathbf{k}$, the sum over $\mathbf{G}$ is usually truncated to include only those plane waves that have a kinetic energy $E_{kin} = \frac{1}{2}(\mathbf{k}+\mathbf{G})^2$ less than a given energy cut-off $Ecut$. The choice of $Ecut$ determines the accuracy of the calculation. More technical details on the plane waves expansion of wavefunctions, charge density and potentials are given in Appendix A.

1.4.2 Brillouin Zone sampling: the use of Γ point

The computation of the electronic density, and then of the total energy, requires an integral over the BZ: $n(\mathbf{r}) = \sum_{\mathbf{k}\in BZ} w_{\mathbf{k}} \sum_n f_{n,\mathbf{k}} \mid \psi_{n,\mathbf{k}}(\mathbf{r}) \mid^2$. In principle, the sum over the BZ would require an infinite number of calculations for every $\mathbf{k}$-point. This is of course not possible to accomplish in practice, and only an appropriate small number of points are considered in the sum. If these are chosen according to precise symmetry criteria, a rapid convergence of the sum can be achieved. Sets of special $\mathbf{k}$-points have been computed [37,38,39] for supercells with different symmetries (simple cubic: SC, face centered cubic: FCC, etc.).

If only the single point $\mathbf{k}$=(0,0,0), i.e. the Γ point is considered,

the wavefunction has the periodicity of the cell. In order to include components of longer wavelengths, k-points other than Γ need to be introduced or, alternatively, the size of the cell has to be increased.

Let us consider, as an example, a Silicon crystal described by the unitary SC cell containing 8 atoms: if the Γ point only is used for sampling the BZ, the diamond structure is not found to have the lowest energy. The use of the Baldereschi point [37], $\mathbf{k} = (\frac{1}{4}, \frac{1}{4}, \frac{1}{4})$, allows instead for an accurate description of the structural properties of the crystal (the computed lattice parameter is within one percent of the converged value and in good agreement with experiment [40]). However a similar accuracy can be obtained by using only Γ within a larger supercell containing 54 atoms [25].

We note that a source of computational saving in BZ sampling with special points is the symmetry of the crystal. Following the previous example, a single calculation with the Baldereschi point provides a sampling of the 8 k-points contained in the corresponding star. However, for a general lattice distortion, the point-symmetry of the lattice is broken. Therefore, to the purpose of computing finite temperature properties in MD simulations, the symmetry of the BZ is not a substantial aid and the use of the Γ point with large supercells appear to be the most efficient choice.

We finally point out a computational advantage in using the Γ point: since the phase of a wavefunction is arbitrary, at Γ this can be chosen to be real. The symmetry $c(-\mathbf{G}) = c(\mathbf{G})^*$ can be used to reduce the Fourier components, i.e. the basis set, of a factor of two.

1.4.3 Core-Valence electrons interaction: first principles pseudopotentials

As mentioned in parag. 1.2, the potential operator $\widehat{V}^{ext}$ which describes the interaction between the ionic cores and the valence electrons is expressed as a sum of ionic pseudopotentials:

$$\widehat{V}(\vec{r}) = \sum_I \widehat{v}_{ps}(\vec{r} - \vec{R}_I) \tag{1.13}$$

In the formulation proposed by Hamman Schluter and Chiang [14] (hereafter referred to as HSC), $\widehat{v}_{ps}$ is a norm-conserving, angular momentum dependent pseudopotential, obtained from first-principles atomic computations. Its explicit form $\widehat{v}_{ps}$ is:

$$\widehat{v}_{ps}(\vec{r}) = \sum_{l=0}^{\infty} v_l(r)\widehat{P_l} \tag{1.14}$$

where $\widehat{P_l}$ is the projector onto the l-th angular momentum. For most elements of the periodic table, it is a good approximation to assume $v_l(r) = v_{\bar{l}}$ for $l \geq \bar{l}$, where $\bar{l}$ is taken to be either 1 or 2. In the former case, s-only non locality is included in the total pseudopotential, whereas in the latter, (s+p)-non locality is included. Eq. 1.14 becomes:

$$\widehat{v}_{ps}(\vec{r}) = v_{local}(\vec{r}) + \sum_{l=0}^{\bar{l}-1}[v_l(r) - v_{\bar{l}}]\widehat{P_l} \tag{1.15}$$

The second term on the right hand side is called the semilocal part of the pseudopotential (V_{SL}): the term semilocal indicates that V_{SL} acts in a different way on different angular components of the wavefunctions (and in that it is non local), but it is a multiplication operator, as far as the radial part of the orbitals is concerned. $\Delta v_l(r) = [v_l(r) - v_{\bar{l}}]$ is the radial part of $\widehat{v}_{ps}$, which is a short ranged function, usually expressed as a sum of a small set of gaussian-type functions ($exp(-a_i r^2)$ and $r^2 exp(-a_i r^2)$, $i = 1, 3$). The matrix element of V_{SL} between two plane waves of

wavevectors $\mathbf{q}$ and $\mathbf{q}'$ is given by:

$$< \mathbf{q}|V_{SL}|\mathbf{q}' >= 4\pi \sum_l (2l+1)\mathcal{P}_l[cos(\theta_{q,q'}] \int dr r^2 j_l(qr) j_l(q'r) \Delta v_l(r) \tag{1.16}$$

where $\mathcal{P}$ is the Legendre polynomial of order l, j_l indicates a Bessel function of the first kind of order l and $\theta_{q,q'}$ is the angle between the momentum vectors $\mathbf{q}$ and $\mathbf{q}'$. In order to evaluate the contribution to the total energy of the semilocal part of the pseudopotential, $m \cdot N(N+1)/2$ integrals of the kind of those entering in Eq. (1.16) need to be evaluated, where m is the number of $\mathbf{k}$ points used to sample the BZ, and N indicates the number of plane waves adopted for the expansion of the wavefunction. This usually amounts to a very large number of integrals, making the evaluation of matrix elements (1.16) computationally very demanding. The computation of these matrix elements can be considerably simplified if they can be expressed in a separable form:

$$< \mathbf{q}|V_{SL}|\mathbf{q}' >= \sum_l f_l(\mathbf{q}) \cdot g_l(\mathbf{q}') \tag{1.17}$$

where f_l and g_l are appropriate functions, each depending on only one wavevector component. A particularly effective way to accomplish this separability has been proposed by Kleinman and Bylander (KB) [41]. In their formulation, the semilocal pseudopotential V_{SL} is substituted by a fully non local (NL) operator (that is an operator which acts in a different way both on the angular and the radial part of the wavefunction), given by:

$$V_{NL} = \sum \frac{|v_l(r)\Phi_{lm} >< \Phi_{lm} v_l(r)|}{< \Phi_{lm}|v_l|\Phi_{lm} >} \tag{1.18}$$

where $\Phi_{lm} = \phi_l(r) Y_{lm}$ is an eigenfunction of the atomic pseudohamiltonian in which the core-valence interaction is replaced by the pseudopotential v_l. The form of V_{NL} allows to reduce the number of integrals that need to be evaluated to mN and then a considerable reduction

in the computer time required to evaluate the pseudopotential energy and potential. In the calculations which will be presented in the following chapter, the fully non local form of the pseudopotential has been adopted. Several computations on tests systems (such as the silicon crystal in the diamond structure and the Si_2 molecule) have shown that the KB pseudopotential give the same result as the semilocal HSC one.

Chapter 2

Thermodynamic properties of crystalline silicon

2.1 Introduction

The ab-initio calculation of properties of semiconductors is a central issue in present day theoretical solid state physics. In the last 10 years a major progress has been made with the advent of accurate total energy calculations based on the local density approximation for exchange and correlation within density functional theory (DFT). These calculations have shown that it is possible to predict accurately properties like the equilibrium lattice structure, the elastic constants and the phonon spectrum [13].

However even relatively simple thermodynamic properties like the thermal expansion coefficient,

$$\alpha = \frac{1}{3\Omega}\left(\frac{\partial\Omega}{\partial T}\right)_P = \frac{1}{3B}\left(\frac{\partial P}{\partial T}\right)_\Omega \tag{2.1}$$

where Ω is the volume, P the pressure , B the Bulk Modulus and T the temperature, have not been calculated with ab-initio methods. The basic reason is that α is dependent on anharmonic effects and therefore its evaluation can hardly be reduced to a small set of total energy cal-

culations as has been the case for the properties listed above. Even if one uses the well known quasi-harmonic approximation for α:

$$\alpha = \frac{1}{3B} \sum_{k,s} \frac{-1}{\omega_{k,s}} \frac{\partial}{\partial \Omega} \omega_{k,s} \frac{\partial}{\partial T} \epsilon(\omega_{k,s}, T) \tag{2.2}$$

where $\epsilon(\omega_{k,s}, T)$ is the internal energy of an oscillator of frequency $\omega_{k,s}$ at temperature T, one is faced with the difficult task of evaluating, in the whole Brillouin Zone (BZ), the phonon frequencies $\omega_{k,s}$ and their volume derivative, i.e. the so called Grüneisen parameters. The integral over the BZ can be simplified by the use of sets of special points [37,38,39], but still the calculation of phonon frequencies at such points would be difficult since it requires the introduction of prohibitively large supercells. Such difficulty is circumvented by the use of molecular dynamics methods [8] that take fully into account anharmonic effects and do not require explicit evaluation of the whole phonon spectrum. Since however these methods are based on the classical approximation for the ionic motion, they will correctly determine α only for temperatures T larger than the Debye temperature Θ_D ($\Theta_D \simeq 645K$ for Si), where quantum effects can be neglected. In this limit eqn. (2.2) predicts a temperature independent α.

In this chapter we show that thermodynamic properties of semiconductors are accessible to first principles calculations and can be computed with good accuracy within ab-initio MD simulations. In particular we calculate the thermal expansion coefficient of crystalline silicon at high temperatures with both constant volume and constant pressure MD simulations.

2.2 Constant Pressure MD

In the original formulation of the MD simulation method, the classical equations of motion for N particles in a fixed MD box of volume Ω, are solved numerically. Time averages calculated over sufficiently long trajectories are equivalent to averages over the microcanonical ensemble. In the last decade, a notable effort has been devoted to generalize the MD method to allow for the study of static and dynamic properties of systems represented by different statistical ensembles. The first contribution in this direction is due to Andersen [42]: he suggested a way of introducing volume fluctuations into MD simulations which allows to describe a system in the isoenthalpic-isobaric ensemble. Subsequently, Parrinello and Rahman [43] modified the Andersen's formulation so as to allow for changes not only in the volume, but also in the shape of the MD cell. This new formulation has been successfully applied to study polymorphic transitions in single crystals [44]. Finally, Nosè [35,36] proposed a generalization of the MD method suitable for constant temperature simulations, which has been discussed in the previous chapter.

Here we describe in some detail the Andersen method for constant pressure MD (CPMD), which has been implemented within the first-principles MD scheme. The simulation of a system at constant pressure requires the introduction of volume fluctuations. Therefore the volume in CPMD is treated as a dynamical variable. Following the approach of ref. [42], we added the following terms to the lagrangian in eqn. (1.6)

$$\frac{1}{2}W\dot{\Omega}^2 + P\Omega \tag{2.3}$$

where P is the external pressure imposed on the system, and W is a parameter of appropriate units adjusted to set the time scale for volume fluctuations. The classical equations of motion for the ions and for the

volume derived from this new lagrangian are the following:

$$M_I\ddot{\mathbf{R}}_I = -\frac{\partial E}{\partial \mathbf{R}_I(t)} - \frac{1}{3}M_I\mathbf{R}_I\left[\frac{2}{3}\left(\frac{\dot{\Omega}}{\Omega}\right)^2 - \frac{\ddot{\Omega}}{\Omega}\right] \tag{2.4}$$

$$W\ddot{\Omega} = -\frac{\partial E}{\partial \Omega} + \sum_I \frac{M_I}{3\Omega}\left[\dot{\mathbf{R}}_I - \frac{1}{3}\mathbf{R}_I\frac{\dot{\Omega}}{\Omega}\right]^2 - P \tag{2.5}$$

These equations couple the dynamics of the particles to that of the volume. The equation of motion for the electronic degrees of freedom is unchanged by the introduction of these new terms in the lagrangian. Andersen [42] has proved that the time averages calculated along the trajectories generated by these equations of motion, are equivalent to averages in an isoenthalpic-isobaric ensemble in which the pressure is P.

2.3 Structural T=0 properties and details of the calculation

We used a periodically repeated MD cell with the silicon atoms arranged in the diamond structure. In most of our calculations we used a 54 atom FCC cell and an energy cutoff $Ecut = 8Ry$ for the expansion of the ψ's in plane waves. BZ sampling was performed with the Γ point of the MD cell. The pseudopotential was taken from ref. [15] considering only s-nonlocality and using the Kleinman-Bylander representation [41]. We have checked the convergence of our results by making additional static and dynamic calculations with larger energy cutoffs and including p-nonlocality. The dependence of our data on the MD cell was investigated by repeating some of the calculations with a larger 64 atom SC cell. In all our calculations we have kept fixed the number of plane waves (N^{PW}) when varying the volume of the cell (we used N^{PW} as defined by the theoretical equilibrium volume at a given Ecut). This gives rise to a slower convergence with respect to cutoff, than working at fixed

	$T=0$ lattice param.(a.u.)		Bulk mod.(Mbar)	
Experimental	10.263		0.992	
Theory: ref. [46]	10.204		0.93	
Our results: 54 at. FCC cell	s-nl	sp-nl	s-nl	sp-nl
$Ecut = 8Ry$	10.00	9.96	1.53	1.32
$Ecut = 12Ry$	10.22	10.09	1.21	1.18
$Ecut = 24Ry$	10.41	10.21	0.89	0.97
64 at. SC cell	s-nl	sp-nl	s-nl	sp-nl
$Ecut = 8Ry$		9.92		1.35
$Ecut = 12Ry$		10.04		1.20

Table 2.1: Convergence study of equilibrium lattice constant and bulk modulus of crystalline silicon. Our results are obtained from pressure calculations within a constant N^{PW} procedure, as in ref. [46,47,48]. The experimental values and the theoretical results of ref. [46] are also presented for comparison.

Ecut [45]. However in our MD simulations, particularly at constant pressure, we are forced to adopt a fixed N^{PW} scheme.

The results of our static convergence tests, for the lattice parameter and the bulk modulus B at T=0, are reported in Tab. 2.1.

The main factor affecting the convergence of our results is Ecut, while a better sampling of the BZ as done in ref. [46], has only minor effects. These results give a strong evidence that the Γ point works well with sufficiently large supercells. Indeed our 24 Ry calculation compares well with that of ref. [46] when we include p-nonlocality (sp-nl), whilst using only s-nonlocality (s-nl) we overestimate the bond length by $\simeq$ 2%. Similar conclusions on the effect of p-nonlocality were obtained in ref. [49].

The integration of the equations of motion was made with the Verlet algorithm [28] using a fictitious mass $\mu = 300$ a.u. and an integration time step $\Delta t \simeq 1.7 \times 10^{-16} sec.$ Such a value is only a factor ~ 2 smaller than the Δt used for instance by Broughton et al. [50,51] in a

conventional MD simulation for silicon based on empirical interatomic potentials.

We performed two kind of simulations, one at constant volume (CVMD) and the other at constant pressure (CPMD) [42]. In our simulations we set $P = 0$ and took $W = 0.05$ *a.u.*. In every run the system has been heated up and then has been equilibrated for at least $500\Delta t$ before taking cumulative averages. An analysis of the data showed that, for the quantities of interest, $3000\Delta t$ were sufficient to compute accurate averages.

2.4 Thermal expansion of c-Si

In order to check that the BO dynamics can be evaluated correctly from the lagrangian (1.6), we have calculated the internal energy of the system as a function of temperature. We calculate the ionic internal energy as

$$U_I'(T) =< \sum_I \frac{1}{2} M_I \dot{\mathbf{R}}_I^2 + E[\{\psi_i\}, \{\mathbf{R}_I\}] > \qquad (2.6)$$

where the angular brackets indicate temporal average on a convenient finite observation time, and the (ionic) temperature T is related to the equilibrium value of the kinetic energy $< K_I >=< \sum_I \frac{1}{2} M_I \dot{\mathbf{R}}_I^2 >$ by suitable normalization. In the hypothesis of adiabatic behaviour of the coupled dynamics for $\mathbf{R}_I$ and ψ's during the observation time, $U_I'(T)$ as defined in eqn. (2.6) should be a good approximation of $U(T) =< \sum_I \frac{1}{2} M_I \dot{\mathbf{R}}_I^2 + \Phi(\{\mathbf{R}_I\}) >$. For a classical highly harmonic system, which is the case here, $U(T)$ is given by the equipartition law : $\Delta U(T) = U(T) - U(0) = N k_B T$, where k_B is the Boltzmann constant and N is the number of degrees of freedom of the (ionic) system. It is seen in Fig. 2.1 that this is indeed the case and that CVMD and CPMD give

consistent results. This result provides further evidence that the electronic degrees of freedom follow the ionic motion without acquiring a significant kinetic energy. In MD simulations the thermal expansion co-

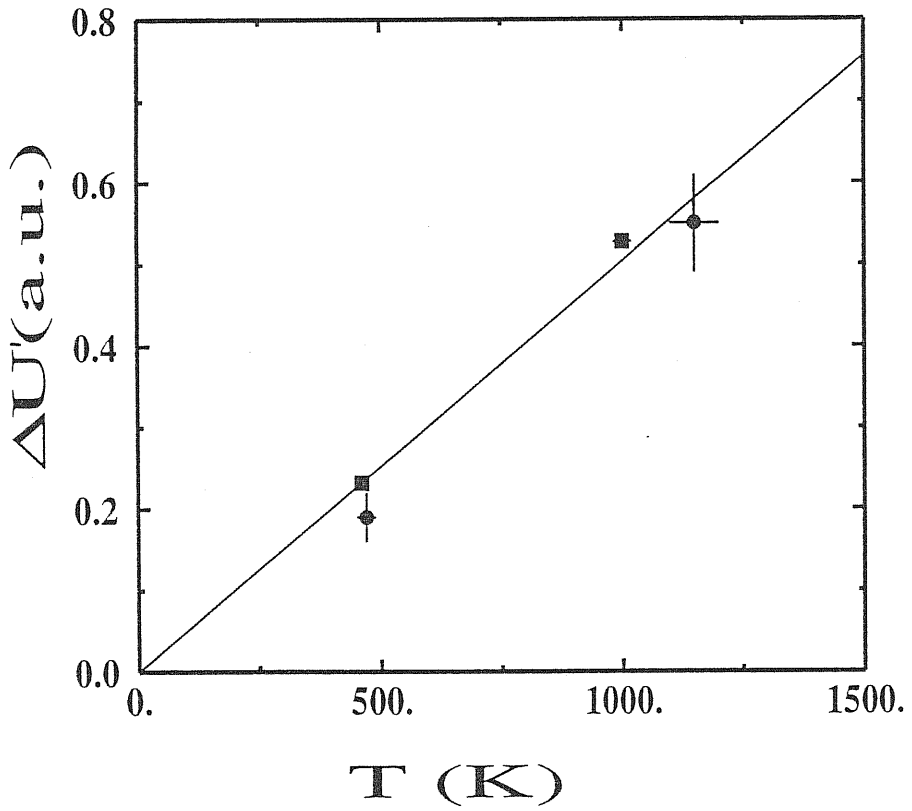

Figure 2.1:
Variation of the internal energy U_I' of crystalline Si with temperature. Results of both CVMD (solid squares) and CPMD (solid circles) are displayed. Horizontal and vertical bars are error bars. The exact result for a classical harmonic crystal is represented by the straight line

efficient can be computed directly from the definition $\alpha = \frac{1}{3\Omega}\left(\frac{\partial \Omega}{\partial T}\right)_P$ or $\alpha = \frac{1}{3B}\left(\frac{\partial P}{\partial T}\right)_\Omega$ if CPMD or CVMD are used, respectively. The derivatives are calculated numerically by making a finite temperature change ΔT, either at constant P or at constant Ω, with respect to a reference equilibrium thermodynamic state, which we have chosen to be the state

at T=0, P=0. This is adequate even at high T since we found that both Ω and P vary linearly with T within the accuracy of our calculations, confirming the prediction of the classical quasi-harmonic theory. Notice that both Ω and B vary little with T: for instance, Ω changes by about 1 percent for $\Delta T \simeq 1000K$. The results of our calculation are displayed

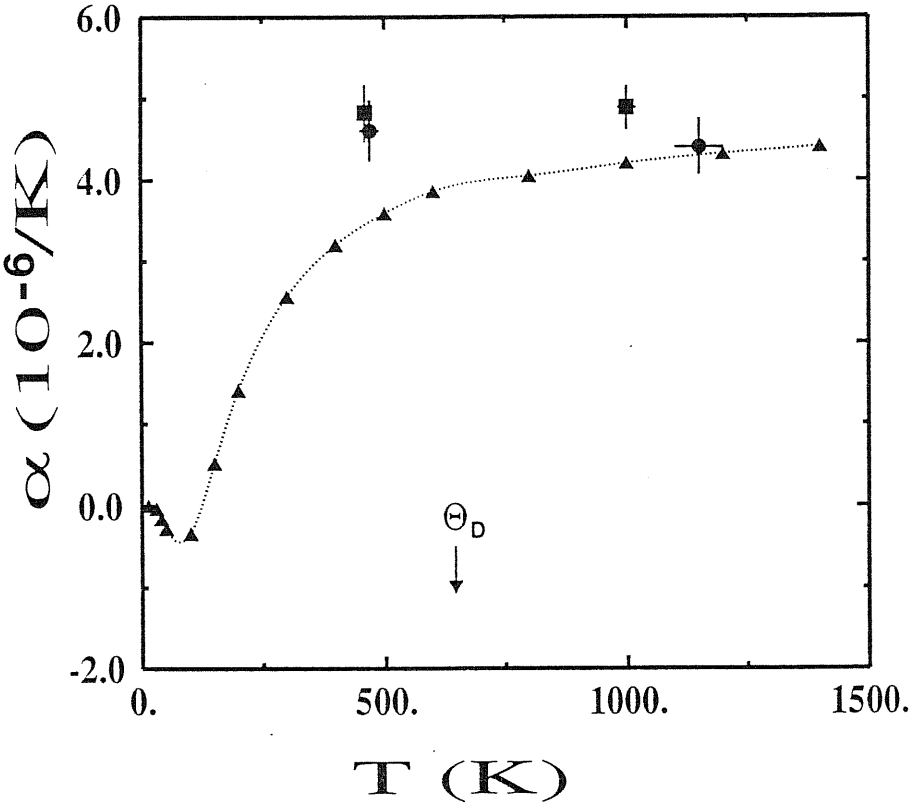

Figure 2.2:
Thermal expansion coefficient α of c-Si as a function of temperature. Experimental values, indicated with triangles, are taken from ref. [52]; the dotted line is just a guide to the eye. Theoretical values: squares and circles indicate CVMD and CPMD results respectively. The error bars are also shown. The Debye temperature Θ_D is indicated by the arrow.

in Fig. 2.2 together with the experimental curve. The experimental data show for $T < \Theta_D$ a rich structure which includes at low temperatures

	$\alpha \times 10^{-6} K^{-1}$	
Experimental ($T \geq \Theta_D$)	$3.9 \div 4.4$	
SW potential: ref. [51]	2.0	
Our results: 54 atoms FCC cell	s-nl	sp-nl
$Ecut = 8Ry$	4.9	4.4
$Ecut = 12Ry$	5.6	4.5
64 atoms SC cell	s-nl	sp-nl
$Ecut = 8Ry$		3.1
$Ecut = 12Ry$		3.4

Table 2.2: Thermal expansion coefficient α of c-Si. Our results are compared with the experimental values for $T \geq \Theta_D$. The theoretical data are from runs at different T in the range $400 \div 1100K$. The result obtained in a computer simulation using the classical Stillinger-Weber (SW) potential (ref. [51]) is also shown.

also a region of negative expansivity. This behaviour of quantum nature is completely missed by our classical calculation which predicts an approximately constant α. Therefore our data should be compared with experiment only in the high temperature range ($T > \Theta_D$). Already with a cutoff of 8 Ry there is a satisfactory agreement between theory and experiment. Furthermore constant pressure and constant volume data are consistent.

We have checked the stability of our calculation with respect to N^{PW} (Ecut) and the size of the MD box. We have also studied the effect of the inclusion of p-nonlocality in the pseudopotential. In Tab. 2.2 we summarize our results.

These calculations were performed with CVMD simulations because they are slightly less expensive computationally than CPMD (by about 10%).

As to the effect of Ecut we note that the variation from 8 to 12 Ry is

not dramatic expecially when also p-nonlocality is included. Although the full convergence in the T=0 properties is reached at larger Ecut, in the evaluation of α there is a compensation between the variation of B and of $\partial P/\partial T$ with Ecut. Therefore the result at 8 Ry can be considered satisfactory even though not fully converged.

The second point that we considered, is the importance of a more accurate treatment of the non local part of the pseudopotential with the inclusion of both s- and p-nonlocality (sp-nl). From Tab. 2.2 we see that α is quite sensible to p-nonlocality especially for the highest Ecut (there is a reduction of 20%), and the agreement with experiment is improved.

Another important feature that one would like to investigate is the dependence of our results on the MD cell. Since computer limitations do not allow at present an extensive study of the size dependence of our simulations, we have only repeated some of the calculations with a 64 atom SC cell. On going from the 54 to the 64 atom cell the variation of the T=0 structural properties is very small, while the variation of α is not negligible (more than 20%) and results in a somewhat worse agreement with experiment. We suggest that this is a consequence of the different representation of the phonon spectrum that is achieved with the 54 FCC and with the 64 SC cell respectively. While the FCC cell samples only phonons in the interior of the diamond BZ, the SC cell samples several zone-boundary phonons which have the largest negative Grüneisen parameters [52]. This leads to a reduction of the calculated α values (Tab. 2.2). For comparison we also show in Tab. 2.2 the result of a recent calculation of α based on the Stillinger-Weber empirical potential, which leads to a significantly larger underestimate of α [51].

2.5 Conclusions

In this chapter we have presented an ab-initio MD simulation of c-Si at finite temperature. This study indicates that thermodynamic properties of semiconductors are accessible to first-principles calculations.

We implemented the scheme of Andersen [42] for constant pressure MD, within the original approach for ab-initio MD simulations.

By using both constant volume and constant pressure MD simulations, we calculated the thermal expansion coefficient at high temperature. Consistent values and in good agreement with experiment were obtained in the two cases.

Finally, this work provides further evidence of the feasibility of a classical adiabatic dynamics for the ions.

Chapter 3

H diffusion in c-Si

3.1 Existent results

In our thesis we are interested mainly in understanding the microscopic mechanisms for the diffusive properties of H in c-Si. This represents a basic achievement toward a more profound insight of the phenomena associated with hydrogen incorporation in silicon. Therefore, in this section we discuss the existent experimental and theoretical results directly or indirectly related to this issue.

3.1.1 Experimental analysis and results

The behaviour of hydrogen in c-Si has been the object of extensive experimental investigations because of its technological importance, arising mostly from the ability of H to passivate defect-related states [1]. A variety of techniques have been used so far both to realize the incorporation of H in the crystal, and to subsequently investigate its electronic, structural and dynamical properties. The aim of this paragraph is to critically review the principal experimental techniques used so far, and to discuss the most important results.

In order to investigate the behaviour of H in Si the first step is to realize its insertion into the crystal. The two main techniques used for

this purpose, are the exposure of the sample to hydrogen (deuterium) plasma, and the ionic implantation. In the first technique the plasma is excited from H_2 (or D_2 in case of deuterium implantation [53]) gas by using low frequency ($\sim 30KHz$) or radio frequency power coupling [54,55,56,57,58]. The H^+ implantation is instead obtained bombarding the sample with ion beams with energies ranging from < 1 keV [59], to $10 \div 13$ keV [60,67], or even $50 \div 100$ keV [57,61]. The use of the second technique gives rise (expecially for the highest implantation energies) to a large amount of damage in the surface and near-surface of the sample. This fact could make the interpretation of the results somewhat difficult. It has to be mentioned that in the pioneering work of Van Wieringen and Warmoltz [62] (VW), hydrogen was inserted via permeation of H_2 gas at high temperature. It has also to be noted that quite often unwanted presence of H in crystals is due to unintentional insertion during simple cleaning or fabrication processes (such as boiling in water etc.) [1].

Many techniques have been used both to detect the presence and to study the behaviour of H (D) in c-Si. Some of them reveal directly the presence of H (D), others study the variation of the electronic properties of the material after hydrogen insertion. Among the first type we will mention Secondary Ion Mass Spectroscopy (SIMS) and ion channeling, between the others: Deep Level Transient Spectroscopy (DLTS), and capacitance-voltage (C-V) measurements [63,59]. Almost all the techniques that look to the variation of the electronic properties of the material after H insertion are based on the capability of H to neutralize defect-related states. DLTS in particular looks at the ability of H to passivate metal-center related (deep) states.

For a comprehension of structural and dynamical behaviour of H in c-Si the experiments have tried to answer two essential questions: where H (D) is preferentially located in the host lattice, and what is the dif-

fusion coefficient D of this defect inside the material. Knowledge of the detailed lattice location is of crucial importance for the understanding of hydrogen-defect interactions. The first evidence of Si-H_i-like centers in c-Si has been obtained by means of infrared measurements of H (D) implanted at 80 K [61]. Different groups [65,66] attempted to extract from the lines appearing in these infrared spectra, information on H location in c-Si.

The only technique able to observe the deuterium location in c-Si is ion-channeling. This technique have been employed the first time by Picraux and Vook [67] in 1978. Implanting deuterium (D) at 13 keV in a single crystal Si at room temperature, the authors found that D was predominantly located in a single interstitial site 1.6Å from a Si atom along the $< 111 >$ antibonding direction. 1.6Å is close to the molecular SiH bond. This "distorted" antibonding site (the geometrical being at $\simeq$ 1.2Å from the Si atom still in the $< 111 >$ direction) will be referred to in the following as the AB site.

Some years later B.B. Nielsen [60,68] used the same technique with an implantation energy of 10 keV at 30 K. The result was that in the as-implanted sample, 80% of D was located close to the bond center (BC) site and the remaining 20% close to the tetrahedral (Td) site. In the same work it is shown that annealing of the sample up to $\approx 200K$ causes a variation of the relative population of near-BC and near-Td sites: The near-Td site increases its population up to $\approx 30 \div 40\%$, and correspondingly the near-BC site decreases down to $\approx 60 \div 70\%$. From these data a clear assignment for the equilibrium site is problematic, even though the BC site appears the most likely. This difficulty arises mainly from the damage induced by the implantation and the consequent presence of defects (as vacancies) which can trap H.

Recently Kiefl et al. [69] have demonstrated that anomalous muo-

nium in c-Si is located at the BC site. From our knowledge this is all what is known on experimental determination of H (D) location in c-Si.

More efforts have been devoted to measure the diffusion coefficient D of hydrogen in c-Si. Van Wieringen and Warmoltz [62] in their work analyze the behaviour of the diffusion of H in c-Si at high temperatures. The measurements have been made using a simple permeation technique. An H_2 gas was inserted in a permeation cell made by a single silicon crystal. The temperature was kept fixed at a high value with very good accuracy. The presence of H after the passage through the permeation cell was revealed by using a mass spectrometer. Hydrogen showed a very high mobility with a diffusion coefficient $D \simeq 2 \times 10^{-4} \mathrm{cm}^2/\mathrm{sec}$ at $\mathrm{T} \simeq 1470$ K. The temperature scan was not very large, running from 1245 K up to 1480 K. In spite of that it was quite evident that the diffusion of H was exhibiting a typical Arrhenius behaviour, from which the authors were able to extract an activation energy of $0.48eV$ within a 10% error. Molecular diffusion was discarded analyzing the dependence of hydrogen permeation from pressure at the entrance wall. Although the charge state of the diffusing species was not clear, they concluded that, at the investigated temperatures, hydrogen consists mainly of neutral atoms or protons.

Other estimates of the diffusion coefficient of deuterium can be made using SIMS. By a temporal analysis of the depth profiles and by fitting the data in terms of gaussian diffusion, one is able in principle to extract a value for D. The authors of ref. [70], by using a scheme of this type, analyzed a large amount of SIMS data and extracted activation energies much larger than that of VW. In particular an extension of the Arrhenius plot of VW to room temperature gives values that are 7 order of magnitude larger than the prediction of ref. [70] for diffusion of D^+ at the same temperature and 10 order of magnitude larger than that

predicted for D. These differences are at least puzzling.

A completely different approach to measure the diffusion coefficient of H is to take advantage of its capability to saturate defect-related states. In ref. [54], DLTS spectra (together with Thermally Stimulated Capacitance (TSCAP) scans) of deep gold donor and acceptor levels in silicon have been measured. Hydrogen was inserted through exposure to radiofrequency hydrogen plasma. Assuming that H diffusion is proportional to the deactivation of Au centers and having from DLTS spectra the depth profile of Au levels, the author of ref. [56] was able, using a scheme similar to that previously traced for SIMS, to estimate the values of D for a very large temperature range. These estimates are once again much lower than that predicted by the Arrhenius plot of VW. A possible explanation for this difference is the fact that hydrogen can be trapped in the material by impurities other than Au. This quantity of trapped hydrogen is not taken into account in the analysis of ref. [56]. It is clear from the fig. 3.1 that is very hard to extract a single Arrhenius behaviour from data in ref. [56].

Recent C-V measurements [63,59] determined the value of H diffusion in c-Si [63] and in Schottky metal-insulator-semiconductor capacitors [59]. The insertion of H was obtained by wet chemical etching technique in ref. [63] and more conventional exposure of the sample to low energy ion beams in ref. [59]. After H insertion, C-V measurements were used to profile the electrically active acceptor density. Assuming that H is trapped only by the Boron centers, is not difficult to restore from these profiles the value for the diffusion of H. The fact that the measurements of acceptor levels profiles were performed immediately after the hydrogenation process (called real time detection) allows to a rather accurate estimates for D. Both measurements agree well with the extrapolation at room temperature of the VW data. In the experiment

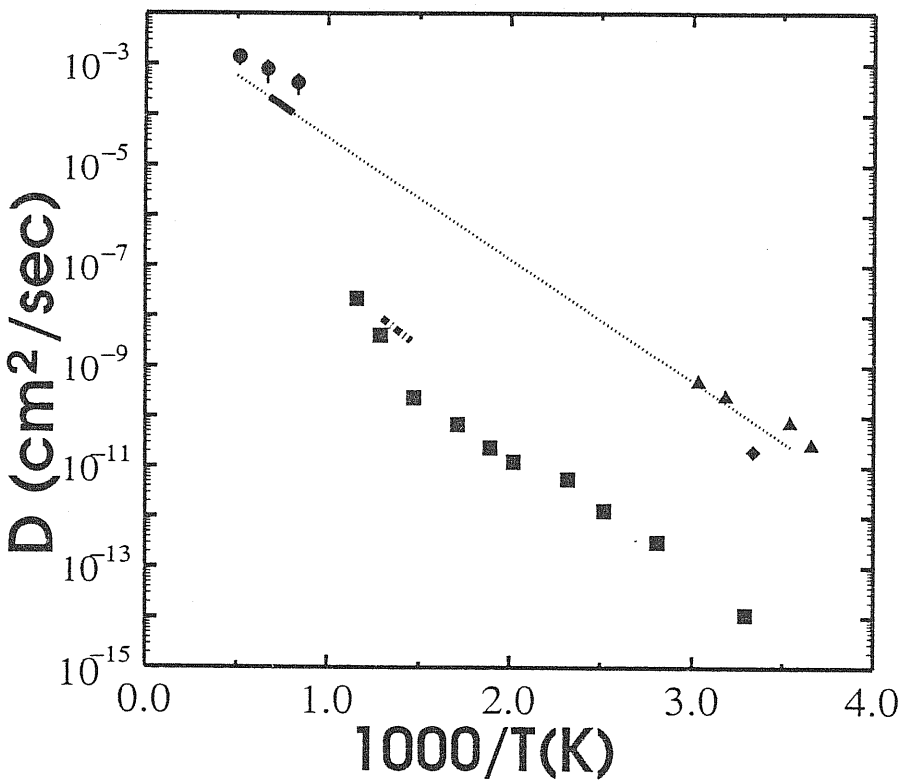

Figure 3.1:
Diffusion coefficient for hydrogen in c-Si as a function of inverse temperature. Solid circles: present calculation for H^+. Error bars are indicated by vertical bars. Solid line: $D = 9.41 \times 10^{-3} \exp(-0.48\ \mathrm{eV}/k_B T)\ \mathrm{cm}^2\ \mathrm{sec}^{-1}$ as obtained by VW (see text) in the temperature range $1240 \div 1480$ K; extrapolation outside this range is given by the dotted line. Dash dotted line: $D = 4.2 \times 10^{-5} \exp(-0.56\ \mathrm{eV}/k_B T)\ \mathrm{cm}^2\ \mathrm{sec}^{-1}$ tritium diffusion from data in the temperature range $670 \div 770$ K [64]. Squares: experimental data from ref. [56]. Diamond: experimental measurement at room temperature from ref. [63]. Triangles: experimental diffusivity values in Au Schottky barrier sample [59].

of ref. [59] a temperature scan from $330K$ to $270K$ was performed. Due to large error bars in the data and the quite short temperature scan, it was not possible to estimate a value for the activation energy of the process. Very recently Jaworowski [71] reported that short term reverse bias annealing at 400 K allows for a real time in-situ measurements of hydrogen migration in the near-surface of silicon. This work further confirms that the fast migrating hydrogen species is H^+; the estimated value of the diffusion coefficient at 400 K is again comparable to the value obtained by extrapolating to 400 K the VW data.

These recent measurements [63,59,71] seems to indicate that a single Arrhenius behaviour can be traced from room temperature up to high temperature ($T > 1200\ K$).

3.1.2 Theoretical approaches and results

In the last few years a very large amount of theoretical work has been devoted to a comprehension of the properties of hydrogen in crystalline semiconductors [6]. In spite of that, due to the complexity of the problem, the ability of theoretical calculations to clarify this issue has been limited and many questions remain open.

It is still debating the quantum nature of the motion of H. If the assumption of classical motion, that will be our forced choice, is justified at quite high temperatures, it has to be instead carefully motivated before of any conclusion on H motion at low temperature. The zero point energy for H^+ sitting in the low density region has been estimated to be $\approx 0.2\ eV$ [72]. No anomaly, due to quantum diffusion, can be found in the behaviour of Arrhenius plot (as in the case of e.g. metal crystal [73,74,75]) due to the large spread in the experimental results discussed above.

Because of technological relevance, related to hydrogen ability to

passivate defect related states, many of the theoretical investigation have been devoted to understand the structural and electronic behaviour of H close to a dopant impurity in c-Si [76,77,78,79]. This subject lies somewhat away from the main thrust of the present work and will not be discussed further.

In pure c-Si the attention of theoretical work has been mostly devoted to predict equilibrium site for an isolated H impurity. This aim can be reached by means of total energy calculations. Two different approaches can be used to compute the total energy surface of a given system: The supercell and the cluster methods. In the first, the energy is computed for a periodically repeated cell containing a number of silicon atoms and one impurity. The use of periodic boundary conditions (pbc), helps in reducing possible surface effects, but introduce a spurious (fictitious) interaction between the impurity and its images. This effect can be removed by using larger cell. In the cluster approach the impurity is surrounded by as many as possible atoms of the host lattice without imposing any boundary condition. The dangling bonds of silicon atoms that remain uncoupled at the surface of the cluster, are usually saturated with H atoms. Different way of saturation may lead to qualitatively different results [84].

The importance of the relaxation of the silicon host lattice has been understood only recently [81,82,83,84]. In spite of the presence in diamond lattice of regions in which the valence electron charge density is quite poor (low density region: LDR), hydrogen prefers to sit at the center of a Si-Si bond (BC site) [81,82,83,84]. In this region there is an high valence electron charge density (high density region: HDR). This minimum in the energy surface is associated with strong relaxation in the silicon lattice ($\approx$ 0.5Å for each neighbouring silicon atom). This founding is the most relevant common feature of all the calculations in

which the Si atoms were free to relax [81,82,83,84].

In the work of ref. [85] a comparison between unrelaxed and relaxed energy surface is presented for H^+. The unrelaxed surface is very similar to that presented by Stoneham and Mainwood [72] and Pennetta [86]. These results show that without relaxations this case the HDR lies very high in energy by respect to LDR.

Although all the papers mentioned above argue that H (H^+) prefers to sit in HDR, the energy differences between HDR and LDR are quantitatively very different. Cluster calculations [84,83,81] overestimate this difference by respect to the supercell method [82,87]. Moreover the fine details of the energy surface in both regions differ from one work to another.

In the rather accurate supercell calculation of ref. [82,85], the authors found the HDR lower by more than $0.5eV$ by respect to LDR, as can be seen in fig. 3.2. On the basis of these $T = 0$ calculations, many authors have tried to extract informations on possible diffusive path followed by H^+ [81,82,83,84]. In particular the authors of ref. [82] predict as the most likely the path connecting adjacent BC sites with the interstitial C site. This path lies entirely in the HDR and requires large and concerted ionic relaxation of the host lattice. The paths lying in the LDR, although requiring negligible ionic relaxation, were discarded as energetically unfavourable.

We want to stress here that it is impossible to infer from static calculations unambiguous information on the dynamical behaviour of H. At finite (high) temperature in fact dynamical effects could significantly modify the picture extracted at $T = 0$. At low temperature instead possible quantum effects of H motion could become important in determine H localization, and have to be carefully evaluated.

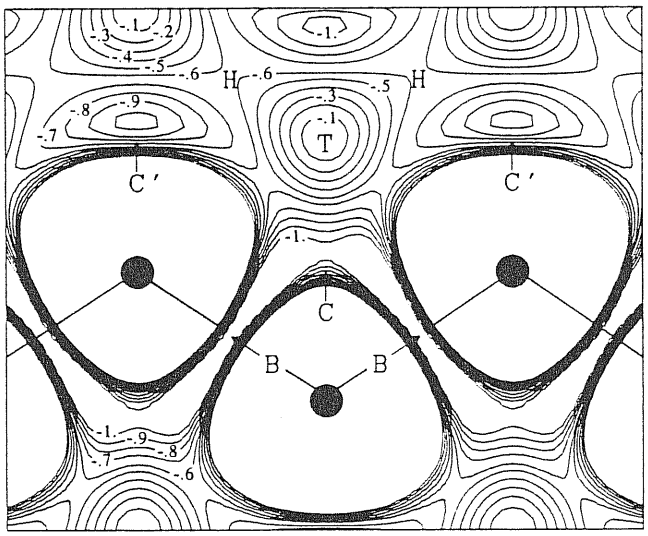

Figure 3.2:
Contour plot in the (110) plane of the total energy surface for H^+ in c-Si [82]. Balck dots indicate atomic positions. The energy difference between adjacent contours is 0.1 eV. the zero of energy is chosen at the tetrahedral site.

3.2 Results of an ab-initio MD simulation

In this section we separately discuss the "static" calculations and the dynamical simulation runs.

Here with "static" we mean total energy calculations performed to investigate the total energy surface for H in the host lattice. We want to stress that the knowledge of this static (zero temperature) energy surface cannot give rise to definitive answers about the dynamics of the diffusion process. Since the diffusion occurs at finite temperature, only including the enthropic and/or dynamical effects we can describe correctly the physics of this process. Therefore a statistical mechanical approach is the most adequate to face with this problem.

However, these static calculations are necessary as the first step because they allow us: (i) to identify the more stable locations for H and the energy barriers between different sites; (ii) to test the convergence

of our results with respect to different parameters of the calculation (size of the MD box, energy cut-off, sampling of the BZ) and then to establish the degree of accuracy of our description of the potential that determines the dynamics. In addition we have the possibility of comparing our results with the total energy surface obtained theoretically in ref. [82,85] where conventional DFT calculations have been performed.

Then we will describe in detail the dynamical behaviour of H for different temperatures pointing out to the importance of dynamical effects on the diffusion process, and we will present numerical results for the diffusion coefficient and the activation energy, making a direct comparison with experimental data.

3.2.1 The SiH molecule: testing and checking the parameters

The study of the SiH molecule can be useful as a first step in the analysis of the accuracy of our calculation in describing both the bonding and the dynamical properties of Hydrogen within a Silicon network. In particular with this test calculation we can investigate: (a) the accuracy of the pseudopotential; (b) the convergence with the energy cut-off ($Ecut$) used in the plane wave expansion of the electronic pseudo-wavefunctions; (c) the choice of the mass parameter μ necessary to have an accurate adiabatic dynamics of the ions.

We consider a SiH molecule in a periodically repeated simple cubic (SC) supercell. The size of the supercell is $20.a.u.$ which is sufficient to have a negligible interaction between nearest images, as we have explicitly tested by using larger supercells, so that the molecule can be indeed considered as isolated.

The interaction between valence electron and pseudoion (nucleus plus core electrons) is described by an *ab initio* norm-conserving nonlo-

cal pseudopotential of the Kleinman and Bylander [41] form constructed from the pseudopotential of ref. [15]. We treat H as purely local, i.e. we use only the s potential (V_s). This potential coincides with the Coulomb potential $1/r$ for $r \geq 0.7a.u.$. For Si we consider s and p potentials. In the Tab. 2.1 we have seen the effect of the inclusion of the d potential (p nonlocality) on the equilibrium lattice constant and bulk modulus of crystalline silicon. We will show that the effect of p nonlocality in the molecule is very small and therefore in the following we will discard this contribution that is instead computationally relevant.

We compute the equilibrium distance d_{eq} and the characteristic frequency ν of the molecule. A study of the convergence of the results with $Ecut$ allows us to establish a reasonable energy cut-off for our purposes.

For the computation of d_{eq} we can relax simultaneously the atomic coordinates and the electronic degrees of freedom. In this simple case there is no risk of being trapped in local minima and therefore we can converge to the minimum with a simple SD procedure for both ions and electrons. For the computation of the frequency ν we perform an MD run in which we leave the molecule free to oscillate around its equilibrium position and measure the oscillation period $T = 1/\nu$.

As we discussed in parag. 1.3, the choice of the mass parameter μ becomes essential when performing an MD simulation: we must use a small enough value of μ to keep the two subsystems uncoupled (adiabatic dynamics); at the same time we want to use a reasonably large time step Δt. It is difficult to give some "a priori" criterion for this choice, that has to be done after direct numerical checking of the adiabaticity. We found that a good compromise in this case is reached with the values of $\mu = 200a.u.$ and $\Delta t = 5a.u. = 1.21 \times 10^{-16} sec.$ Note that the mass of H is about an order of magnitude greater than μ.

The computation proceeds in the following steps: (a) we keep ini-

	Experiment	Theory			
		5 Ry	8 Ry	12 Ry	20 Ry
$d_{eq}(a.u.)$	2.87	3.062	3.055	3.061	3.036
$\nu(THz)$	61.2	60.8	53.0	52.6	54.4

Table 3.1: equilibrium distance and vibrational frequency of SiH molecule for different cut-offs.

tially the ions fixed at a distance slightly different from the d_{eq} and take the electrons on the BO surface (in this case the BO potential is simply a curve as a function of the molecular distance); (b) then we start with the dynamics according to the equations of motions 1.7,1.8.

In fig. 3.3 we show the result of one MD run for $Ecut = 8Ry$: the distance between Si and H oscillates around its equilibrium value and correspondently the kinetic energy oscillates with a frequency twice as great. The dynamical behaviour is highly harmonic and the frequency can be computed directly. The results for different $Ecut$ are presented in Tab. 3.1.

We have repeated the calculation for $Ecut = 12Ry$, including also the p nonlocality in the pseudopotential of Si: the result changes of less than 1% both for d_{eq} and ν. The convergence with $Ecut$ is shown in fig. 3.4, where we report the total energy computed at the theoretical equilibrium distance d_{eq}: a full convergence appears to be reached for $Ecut = 20Ry$. In all these calculations ${G_{max}}^V = 2{G_{max}}^\psi$ (see Appendix A). If a different choice is adopted we will explicitly mention this.

The conclusions that we can extract from this analysis are the following: (i) we have determined the most suitable choice for the parameter μ and we have tested that a good adiabatic dynamics can be obtained. (ii) the study of the convergence of the equilibrium distance and of the

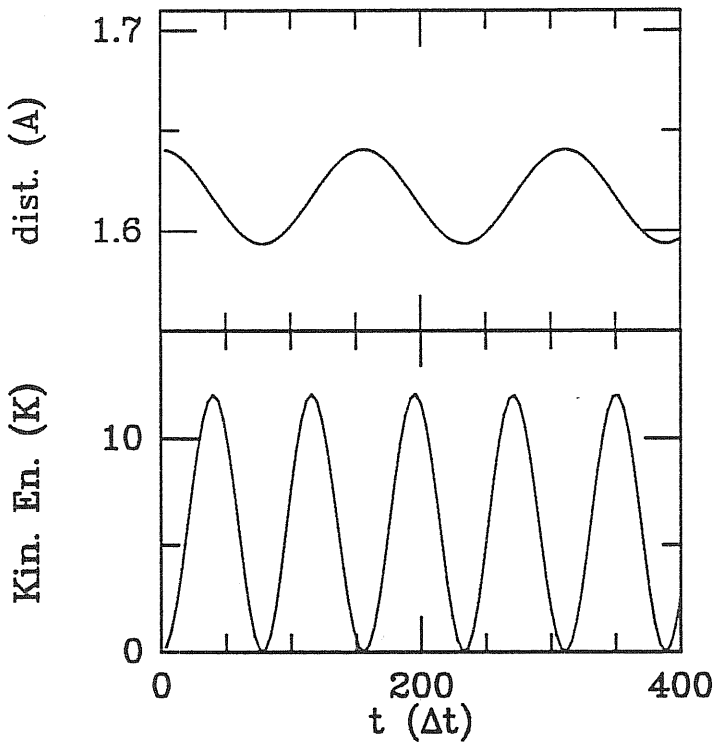

Figure 3.3:
Kinetic Energy (lower part) and intermolecular distance (upper part) as a function of time for SiH molecule.

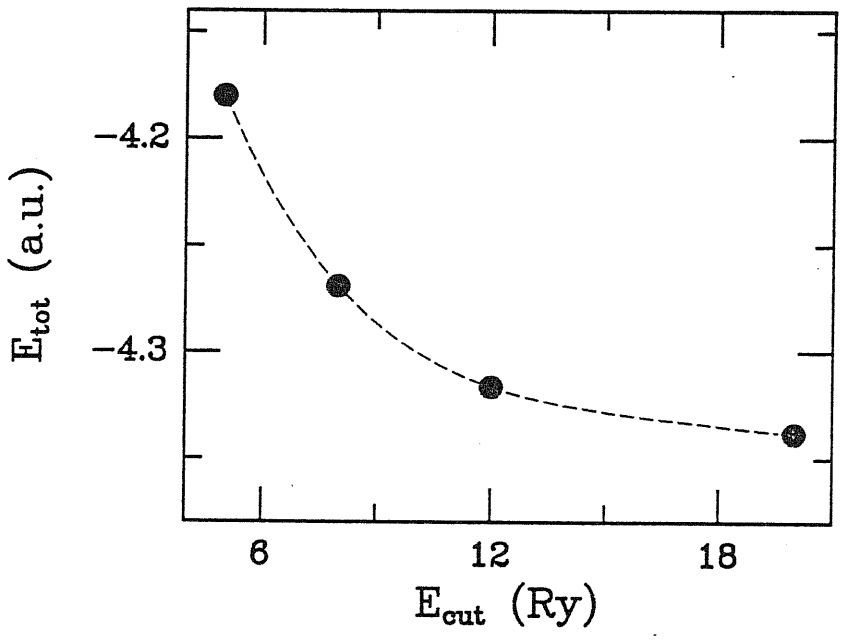

Figure 3.4:
Total energy for SiH molecule at the equilibrium distance as a function of the planewaves cutoff.

frequency with *Ecut*, seems to indicate that a reasonable description of the Si-H bond is obtained already with a cut-off of 5 Ry although a full convergence in the total energy is obtained at 20 Ry. (iii) the effect of the inclusion of the *d* potential for Silicon appears to be negligible.

3.2.2 Static results: details of the calculation and convergence tests

Our final goal is a microscopic understanding of the diffusive behaviour of H in crystalline silicon. Before starting with the dynamics we have to be familiar with the energy surface of H in the host lattice: this energy surface is defined as the potential energy $E(\mathbf{R}_H)$ obtained by putting H in the interstitial lattice position $\mathbf{R}_H$ and allowing all the Silicon atoms to relax. The relaxation is larger for Si atoms close to H impurity, but, for some H location, is appreciable even up to the fourth shell of silicon

atoms (see Fig. 3.5 that we will discuss below). It has been noticed that the host lattice relaxation is essential for having a correct description of the energy surface when H lies in the high valence electron density region (BC, M, C), whereas introduces negligible effects if H sits in the low valence electron density region (Td, Hex) [82,85].

Charge state

As most impurities in semiconductors also H in Silicon can exist in different charge states (H^+, H^0 and H^-). The preferred charge state depends on the doping of the material. Here we focus on the H^+ case that has been argued to be the dominant charge state, at least in p-doped material, both experimentally [88,57,89,59] and theoretically [82]. Because of the BO approximation, the MD-DF method does not allow at present to deal with electron transfer processes, that may switch H^+ into H and viceversa in the actual diffusion process.

Size of the supercell and BZ sampling

As we discussed previously (see parag. 1.4.1) the supercell geometry is a choice necessary to have the periodic boundary conditions (pbc) that are used in MD simulations for bulk. The supercell geometry has become the most used technique in electronic structure calculations, for treating impurities in semiconductors. In contrast with the cluster geometry, in this case surface effects are not present; however the size of the supercell must be sufficiently large to reduce the interaction between the impurity and its periodic images in order that the impurity be considered as isolated. The effect of this fictitious interaction is that the electronic level introduced by the impurity has a dispersion along the BZ of the supercell. Such impurity band dispersion reduces when the size of the supercell is increased, and in the limit of an infinite supercell,

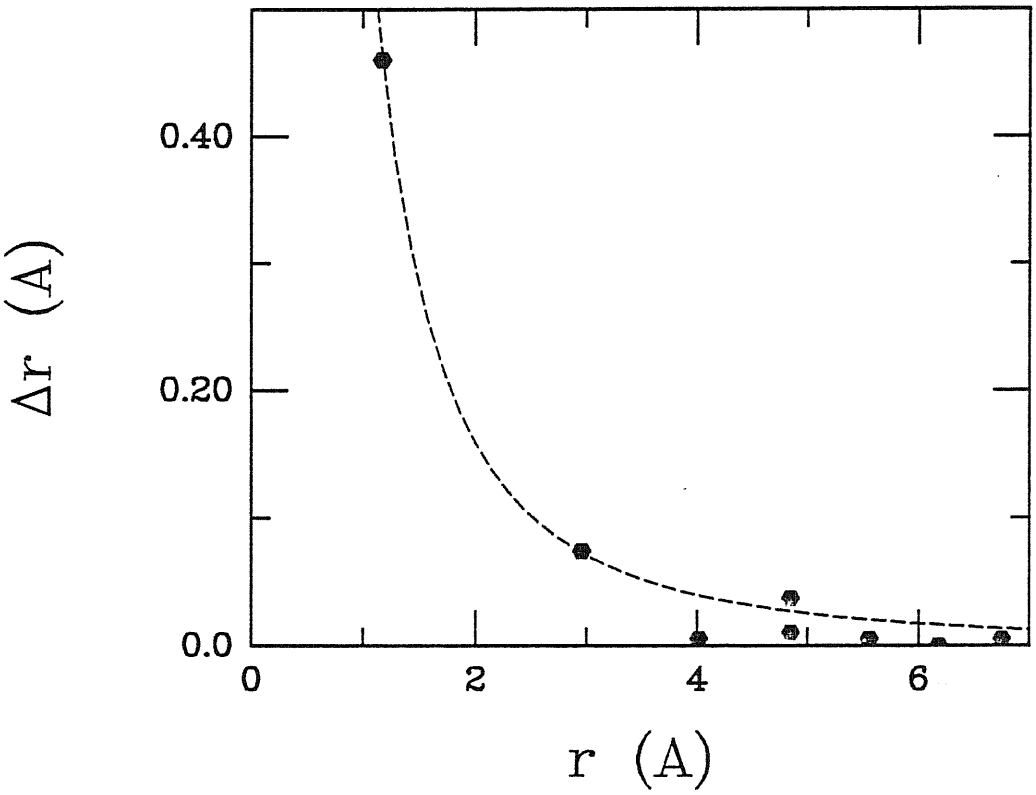

Figure 3.5:
Ionic displacements of Silicon atoms for H^+ located in the BC site vs. shell radius. All the reported shells are complete within our supercell. Dashed Line: $\frac{1}{r^2}$.

disappears. Therefore the problem of treating an impurity within the supercell geometry has two aspects: (i) to treat correctly the interaction between the impurity and the crystal; (ii) to reduce the fictitious interaction between the impurity and its images. The first point is faced sampling the BZ with a larger number of k-points for a given size; the second aspect requires the use of larger supercells. It should be noted that, for fixed k-point, the use of a larger supercell reduces the BZ and therefore at the same time improves the sampling. It is not clear what is the best strategy that reconciles these two aspects and gives the most rapid convergence. We adopted the use of as large as possible supercells using only the Γ point. This choice is also motivated by our purposes that are mainly addressed to study the dynamics of the impurity. Indeed from the point of view of the ionic properties there are several advantages in using large supercells:

(a) one has a better representation of the phonon spectrum in a large system. In a small system with pbc one can only excite a very restricted subset of phonons: in particular phonons whose wavelength is larger than the box size are absent. This point has been also stressed in the previous chapter.

(b) The pbc can be seen as a fictitious constraint imposed on the system. The effect of this constraint becomes negligible if the size of the simulation box is sufficiently large, but can be relevant for very small MD box.

(c) Furthermore the fluctuations in the thermodynamic quantities, like the temperature, scale with the square root of the number of atoms in the MD box; therefore with a larger supercell the host lattice is better described thermodynamically.

In Tab. 3.2 we report the energy difference ΔE between two representative configurations for H^+: the tetrahedral (Td) and hexagonal

	$\Delta E_{Td-Hex}(eV)$		
No. of atoms	k = (0,0,0)		Baldereschi point
(supercell)	6 Ry; $m = 2$	6 Ry; $m = 1$	6 Ry; $m = 2$
32 (BCC)			0.41
54 (FCC)	0.0	0.08	0.41
64 (SC)	0.22	0.27	0.44
128 (FCC)		0.30	

Table 3.2: Energy difference between the Td and Hex configurations for H^+: results for different supercells and k-points are shown; m indicates the ratio between the cut-off used for the potentials and for the wavefunctions, i.e., $m = \frac{G_{max}{}^V}{G_{max}{}^\psi}$.

(Hex) sites. The silicon atoms are not relaxed in this case.

These results show that the use of one special point (the Baldereschi point) is sufficient to have a good convergence in the sampling of BZ already with a supercell containing 32 Silicon atoms. The variation in ΔE is only of 0.03 eV by using a cell two times bigger. The Γ point gives reasonably well converged results when using the biggest supercell we can handle (128 atoms). Note that with the 128 atoms supercell the separation between nearest impurities is of 15.36Å. In this table the effect of using the same G_{max} for wavefunctions and potentials is also shown (see Appendix A) and it will be discussed below.

Plane-wave basis set

We have performed calculations with different energy cut-offs (up to 12 Ry) in the plane wave expansion of wavefunctions, on cells of 32 and 64 Silicon atoms. The variation in the total energy with $Ecut$ can be quite relevant and full convergence would require very large cut-offs ($\approx 20Ry$). However we are interested in energy differences between different H^+ configurations within the crystal: In situations of this kind

at least part of the error due to the truncation of the Fourier series is expected to cancel out and therefore the convergence in the energy differences should be faster.

We found that energy differences between sites in the same region (high or low density) changes by less than 0.1 eV on going from 6 Ry to 12 Ry. When we look at energy differences between sites in different regions, the effect is slightly larger and is such that the energy distance between the two regions is reduced. A cut-off of 6 Ry appears sufficient for having a reasonable description of the energy surface for H^+. A big saving in computing time and in memory can be obtained by adopting the same cut-off in the number of plane waves both for the expansion of wavefunctions and potentials (see discussion in Appendix A). As is shown in Tab. 3.2, in our calculation with 6 Ry, the effect of this approximation is small compared with the error concerning the BZ sampling.

Static results for H^+

From all the analysis and tests discussed so far we concluded that the following parameters are sufficient to describe the energy surface for H^+:

(i) FCC supercell containing 128 silicon atoms. The side of this box is four times the lattice parameter of the silicon crystal ($\simeq 41 a.u.$);

(ii) the Γ point for sampling the BZ of the supercell;

(iii) an energy cut-off of 6 Ry both for wavefunctions and potentials, corresponding to about 5000 plane waves at the Γ point. This number reduces by a factor of two if we employ the fact that the wavefunctions are real at the Γ point.

By using these parameters we calculated the energy of H^+ in different configurations by allowing a full relaxation of the host lattice: within the supercell there are 7 complete shells of silicon atoms that we relax simultaneously. We find the BC position as the energetically

most favourable. In Fig. 3.5 we show the relaxation of all the silicon shells around H located in BC, plotted versus shell radius. The decay of the relaxation amplitudes is compared to a $\frac{1}{r^2}$ behaviour. The relaxation of the two nearest silicon atoms is of 0.46Å outward, so that their distance from H^+ becomes 1.63Å; the second shell including 6 silicon atoms relaxes of 0.07Å; the following shells have a very small relaxation if at all (noticeable the fourth shell including 12 atoms that splits in two subshells of 6 atoms for each with a slightly different relaxation, as visible in Fig. 3.5). By taking the energy at BC as reference, the M site (see Fig. 3.6), also in the high density region, is found to be $\sim 0.15eV$ higher in energy. The relaxation of the two nearest silicon atoms is of 0.20Å outward, and the distance from H^+ is slightly larger than in the BC position. The relaxation of the successive shells is also important for this site. The other highly symmetric site in the high density region is the C site that we found at an energy of 0.32 eV. For the sites AB, Hex and Td, in the low density region, we found respectively 0.54 eV, 0.55 eV and 0.85 eV. The relaxation of the host lattice when H^+ is located in one of these sites is very little and induces a variation in the energy differences of, at most, 0.01 eV. The AB site is not exactly the geometrical one (Q in Fig. 3.6), but it results from a relaxation of H^+ outwards in the direction of the nearest Td site, so that the resulting distance from the nearest Silicon atom is of about 1.6Å, that is close to the molecular SiH bond distance.

Our results for H^+ are overall similar to those obtained in ref. [82]. Although a full convergence in the energy differences would require a more accurate BZ sampling (perhaps Γ within a supercell two times bigger) and higher cut-offs, we can conclude that our energy surface contains all the important features and therefore reliable results can be obtained by the dynamical study. Furthermore, when looking at the

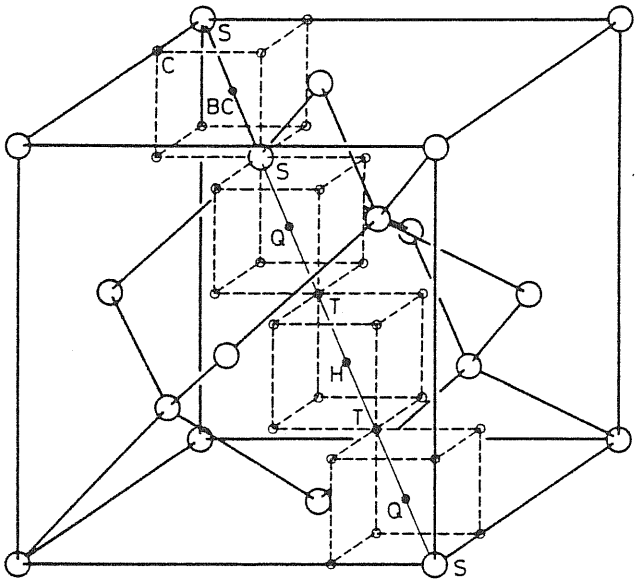

Figure 3.6:
Conventional unit cell of diamond lattice. Various impurity sites are indicated: substitutional (S), bond center (BC), tetrahedral (T), hexagonal (H), geometrical anti-bonding (Q), and C sites. The M sites are located in the middle between two adjacent C sites.

finite temperature dynamical behaviour, details of the energy surface within K_BT are scarcely relevant.

3.2.3 Dynamical results

We studied the dynamical diffusive behaviour of a single proton in perfect crystalline silicon at high temperature ($T \geq 1000K$). This choice relies mainly on two reasons: (i) since we treat the ionic motion classically, we must consider high temperatures where quantum effects should be negligible (we will come back at this point in the following); (ii) the high mobility of H^+ at these temperatures allows to observe, during the finite MD simulation time (typically of the order of few psec), sufficiently long trajectories in order to have a good statistics on the sites visited by the proton during its diffusive motion.

We used a periodically repeated FCC supercell containing 128 silicon atoms and performed microcanonical MD simulations: in particular the volume of the box was kept fixed at the experimental value at T=0. Therefore thermal expansion effects have been neglected. If we consider that the lattice parameter of c-Si varies only by less than 1% at 1000 K, and the ionic relaxation when H sits at BC is 10% of the bond length, we can argue that indeed the thermal expansion effects do not induce important changes in the diffusive process.

The parameters used for the description of the electronic density and therefore of the BO potential are those described in the previous paragraph. The Verlet algorithm (see Appendix B) has been used for the numerical integration of the equations of motion. The values of the time step and of the mass parameter μ have been chosen as discussed in the parag. 3.2.1 ($\Delta t = 1.21 \times 10^{-16} sec, \mu = 200 a.u.$). With this choice we have verified that the total energy deviates from the Born-Oppenheimer surface by less than 0.03 eV/atom after 4 *psec*, i.e. our largest observation time.

Diffusive paths

Many MD runs have been performed in a temperature range varying from 1000 K to $\simeq$ 1950 K, that would correspond to an overheated crystal. The proton has been initially placed in a highly symmetric site in the low (Td) or in the high electronic density (BC) region. We have verified that the starting condition is irrelevant if one looks the diffusive motion on a appropriate time scale. This point will be clarified in the following. The system has been heated by rescaling the velocities of the particles and then equilibrated at a chosen temperature T. A detailed analysis of the diffusive path of the proton has been performed in all of the simulation runs at the various T.

In Fig. 3.7 we plot an equilibrium trajectory for H^+ at 1200 K. For clarity the vibrational motion of the Si atoms is not reported, but it must be stressed that in our simulation H^+ and Si are dynamically coupled and the Si vibrations play an essential role in the diffusion process.

Before describing the details of the trajectory we want to elucidate some general features:
(a) The trajectory shows that the diffusion occurs by jumps between sites of high symmetry. We can identify two kinds of sites along the proton trajectory: (i) sites where the proton resides for longer time, and (ii) sites that are rapidly visited during a jump process.
(b) Both high- and low-density regions are visited by H^+, at variance with what one could expect by looking only at the T=0 energy surface.
(c) The dynamics of the proton is strongly coupled with that of the silicon atoms.

In Fig. 3.7 two different BC passages are clearly visible involving the atoms labelled 1,2 and 1,3 respectively. In going from the bond 1-2 to the bond 1-3 the proton visits the low-density region (Hex site). A large relaxation of the neighbouring Si atoms is associated with every interbond passage. The effect of the coupled H and Si dynamics appears clearly in the inset of fig. 3.7, in which trajectories of few selected Si atoms and the partial trajectory of the proton, corresponding to the passage through the bond 1-2, have been projected onto the (110) plane formed by atoms 1,2 and 3. The relaxation of the atoms 1 and 2 in correspondence with the passage of H^+ through the BC position is demonstrated by the tails of the Si trajectories in the direction of the bond. A second tail in the trajectory of the atom 1 is due to the subsequent passage of H^+ through the bond 1-3 (not shown in the picture). By contrast the trajectory of the third Si atom shown in the inset, is not affected by a passage of H^+ through an adjacent bond and simply

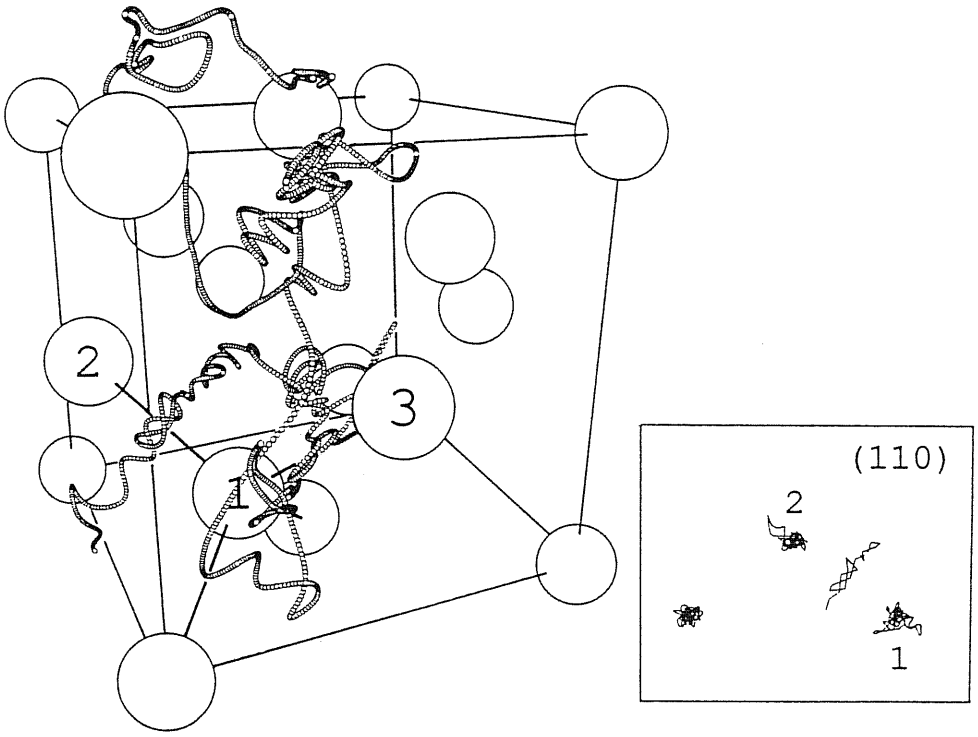

Figure 3.7:
Trajectory of a diffusing H^+ at 1200 K during about 1.5 *psec*. The successive H^+ positions every 6×10^{-4} *psec* are shown by the tiny balls. For clarity we show only a small portion of the total MD cell and draw Si atoms, represented by the large balls, at their perfect lattice positions. The bonds connecting atom 1 to its four neighbours are explicitly indicated.
The inset shows the (110) plane formed by atoms 1,2 and 3 in the main figure. Full projected trajectories of the Si atoms belonging to this plane are reported, while the projected H^+ trajectory is only displayed during $\sim$ 0.2 *psec* corresponding to the passage through the BC position.

reflects the Debye-Waller cloud.

The study of the partial pair correlation function $g_{HSi}(r)$, averaged over different time intervals, i.e. over different segments of the trajectory, allowed us to determine the lattice positions visited by H^+ in its diffusive motion. This is illustrated in Fig. 3.8 where we report a segment of the same trajectory. Again for clarity the thermal motion of the silicon atoms is omitted and only few silicon atoms are reported. In the insets we show the $g_{HSi}(r)$ computed in different segments of the trajectory. The $g_{HSi}(r)$'s corresponding to the passage of H^+ through regions close to the various symmetry sites differ from one another both in their shape and in the coordination shells. For example in the BC position one has the sequence of coordination shells $\{2 : 8 : 20\}$, in the M site one has $\{2 : 16\}$, and for the Hex site obviously the first coordination shell of 6 is recovered. The shape of the $g_{HSi}(r)$ reflects both the hydrogen motion within a particular site and the silicon motion. The first peak of the $g_{HSi}(r)$ in the insets relative to the BC configuration occurs at $\simeq 1.6$Å, indicating an average relaxation of the nearest two silicon atoms of about 0.5Å (that is approximately the relaxation we have detected at T=0). From the sequence of the $g_{HSi}(r)$'s shown in Fig. 2 one can observe that H^+ is moving from a BC site to another one, passing through an M site and an Hexagonal (Hex) site. This shows clearly that the proton follows a path in which it explores alternatively the HD region (BC, M) and the LD region (Hex). However the proton resides longer in the twofold-coordinated sites (BC,M) (e.g. the proton resides near the first BC for about 0.10 *psec*) than in the Hex site (the residence time near Hex is about 0.02 *psec*). This kind of analysis shows again that the diffusion mechanism is jump-like.

It can be noticed that during the motion of the proton from the BC site to the M site, the two nearest silicon atoms relax in such a way that

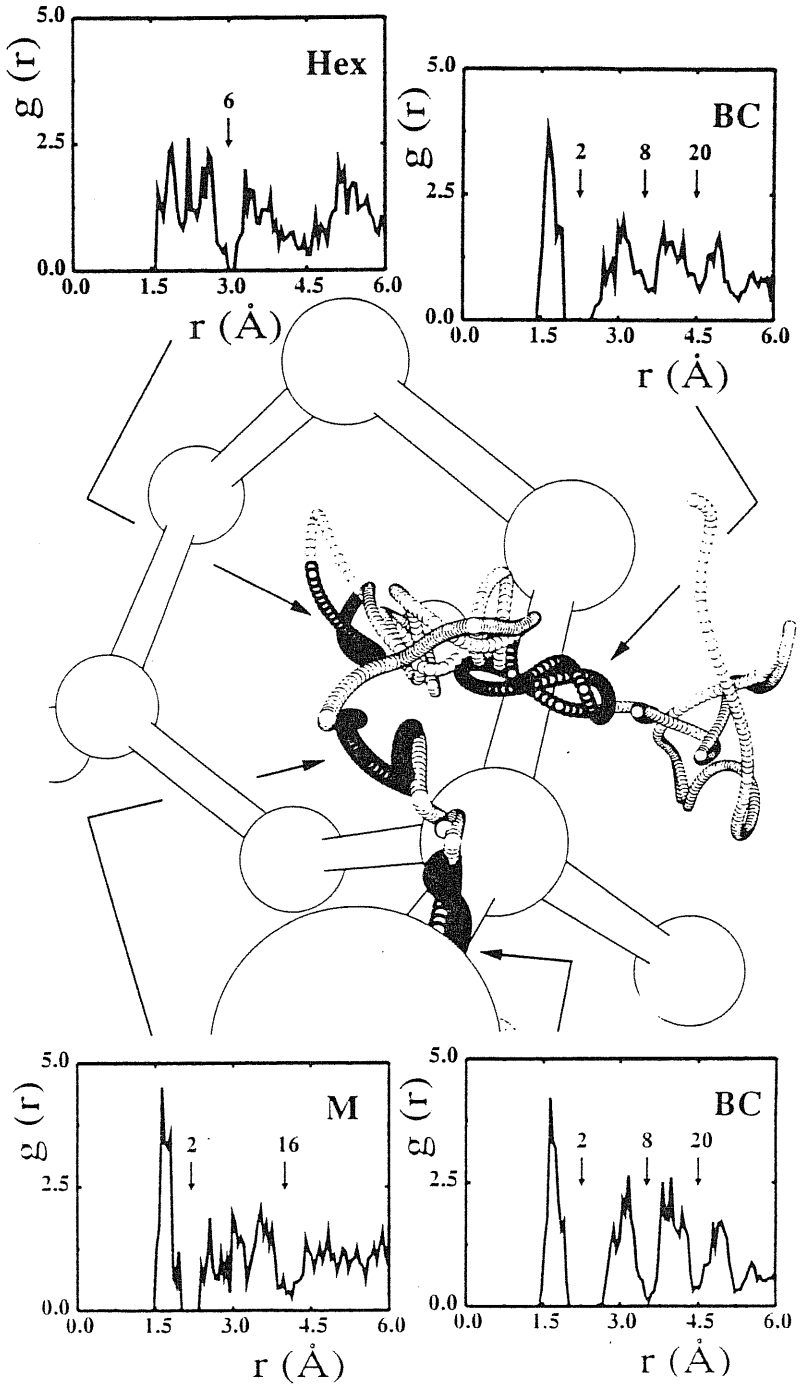

Figure 3.8:
H^+ trajectory at 1200 K for about 0.7 psec. The large balls represent the silicon atoms in the perfect crystalline positions; only few bonds are shown. The small balls correspond to the hydrogen position reported every 5 Δt ($\Delta t \simeq 1.2 \times 10^{-16}$ *sec*). The cross term of the pair correlation function $g_{HSi}(r)$, relative to the passage of H^+ in the darkened regions indicated by the arrows, and the average coordination numbers are reported in the insets.

the average distance from the proton remains approximately constant ($\simeq 1.6$Å). Following the trajectory in fig. 3.7 after the passage through the BC site between atoms 1-3, the proton moves quite rapidly reaching a Td site (visible in the center of the cube displayed in the picture).

More generally we have detected, as the most likely, a path in which the proton jumps from a twofold-coordinated site (BC,M) to another one by using Hex and/or Td as intermediate sites. We will call this path the twofold-coordinated path indicating with this the fact that the proton spends most of its time in twofold-coordinated sites.

In other runs or in different segments of the trajectory within the same run, the proton has been observed to follow a path lying completely in the LD region. In fig. 3.9 we show a portion of a trajectory at about $1000K$ which is an example of this path. This path proceeds more often via jumps from a near antibonding (AB) site (about 1.6Å from a silicon atom) to another one, rotating around a Td site (the dense "tangles" in the trajectory of the figure, located around different Td sites) and more seldom via jumps to a different interstitial region (around a different Td site), using Hex as the crossing site (the segments of the trajectory that connect different "tangles"). In this picture the jump-like mechanism of the diffusion process is particularly evident. Some back-jumps are also visible in this trajectory. We call this the onefold-coordinated path since the proton spends most of its time in onefold-coordinated sites (AB).

The twofold- and the onefold-coordinated paths can alternate during the same simulation run. Indeed we have observed that, on a small time scale (less than 1 *psec*), the initial configuration for H^+ can affect the occurrence of one path rather than the other: In particular, starting from the LD region (Td site) the onefold path seems more favourable, whereas starting from the HD region (BC site) the twofold path occurs more likely. However if we follow the diffusion process for

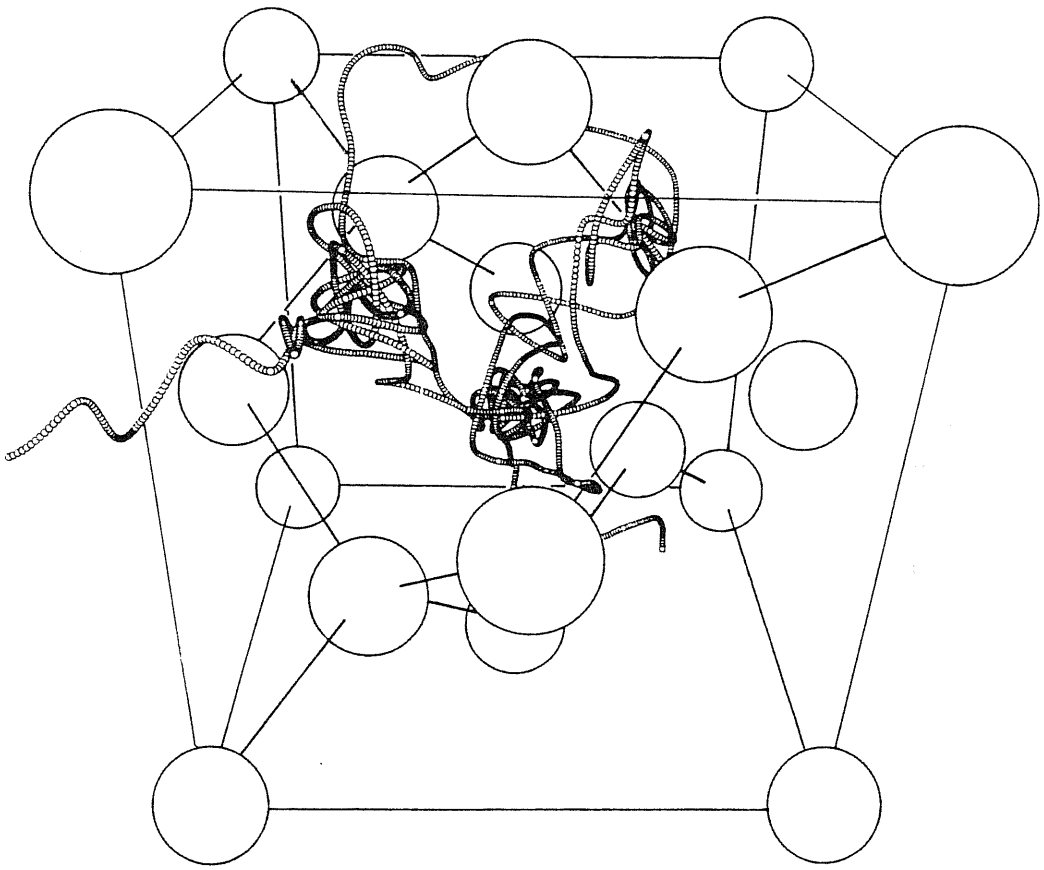

Figure 3.9:
H^+ trajectory at $1100\mathring{K}$ for about $1.9psec$. The large balls represent the silicon atoms in the perfect crystalline positions; only few bonds are shown. The small balls correspond to the hydrogen position reported every 5 Δt ($\Delta t \simeq 1.2 \times 10^{-16} sec$). This represents the so called onefold-coordinated path (see text).

a sufficiently long time ($4 \div 5$ *psec*), we observe that these two paths alternate. Therefore we can assert that the initial configuration of the proton is not essential for the conclusion that we have drawn. We are not able at this stage to give a precise estimate of the relative occurrence frequency of the two paths, although on the base of the statistics accumulated in about ten MD runs, we can state that the twofold path is the most likely.

In conclusion, we have observed that the proton follows diffusive paths that are different from the HD path that is predicted to be the most favourable on the basis of purely T=0 total energy calculations [82]. This demonstrates that, at least at these high temperatures, dynamical effects are very important in determining the diffusion mechanism. The reason of that can be traced to the large mass difference between H and Si. When the H^+ motion is fast, as it is the case at these high temperatures, the heavy Si ions cannot follow adiabatically the proton. Thus the lattice may not have the time to undergo the large relaxation needed for the HD sites to become energetically favourable. When this happens the proton prefers to move through regions of low energy for the undistorted lattice. This explains also the observation of the onefold-coordinated path.

Vibrational density of states

The two paths described above, can be characterized by the relative vibrational frequencies associated to the proton. Indeed these two paths show a significative difference in the velocity-velocity correlation function Z(t) of the proton. We report in Fig. 3.10 the power spectra of Z(t) for H^+ diffusing in the onefold- and in the twofold-coordinated paths, respectively. In the same picture we also show the spectrum computed for silicon which closely reproduces the measured phonon density of states

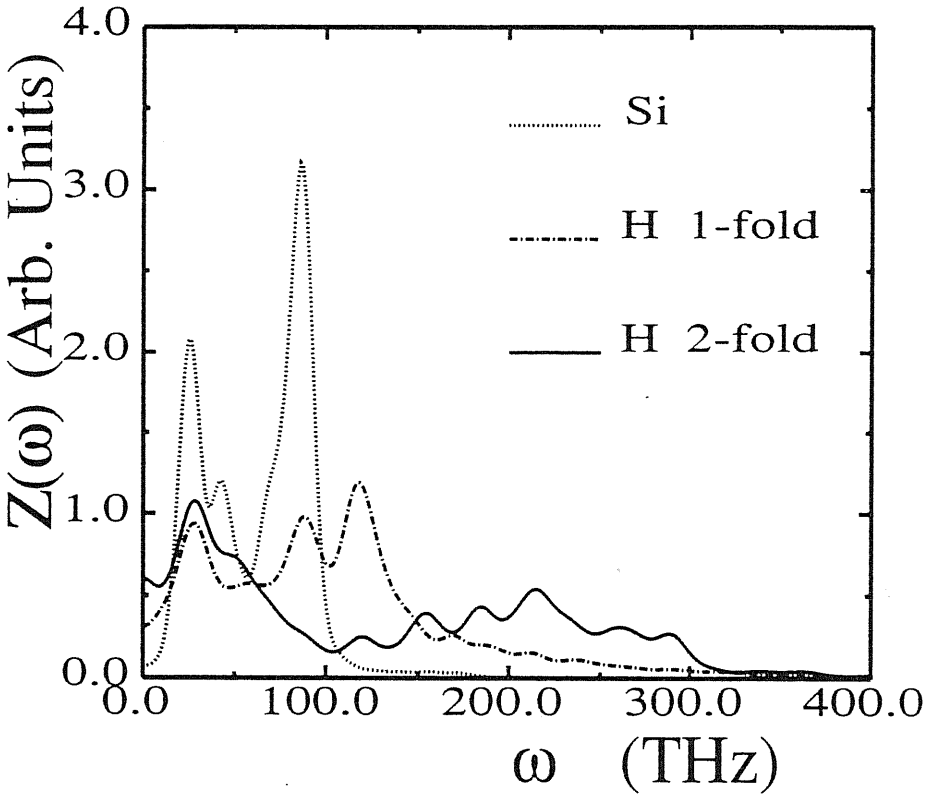

Figure 3.10:
Phonon density of states at $\simeq$ 1000 K. Dotted line: silicon. Dash-dotted line: H^+ in the "one-fold" path (see text). Solid line: H^+ in the "two-fold" path (see text).

of the pure system [90]: In particular the transverse acoustic (TA) and transverse optic (TO) bands are well described.

In the spectrum relative to the onefold path there are three clear peaks: the first two are resonances with the TA and TO modes of the host lattice, the third one occurs at a frequency close to the bending mode of a (Si-H) group [91,92]. Similar frequencies, identified also as bending modes, are observed in a-Si:H [91,92] ($\omega \simeq 119\ THz \simeq 630\ cm^{-1}$). These frequencies could be possibly associated to the motion of the proton in the AB site.

In the case of the vibrational spectrum obtained in the twofold path, higher frequency components appear, whereas the resonance with the TO peak disappears. This is probably related to the fact that the presence of H^+ in BC configuration inhibits the TO excitation in the nearest Si atoms. This fact inhibits the resonance of TO modes in the H^+ dynamics. The highest frequencies ($\omega \simeq 1800 cm^{-1}$) are most likely related to the stretching mode of H^+ in the HD region. In ref. [85] a frequency $\omega \simeq 2200 cm^{-1}$ for H^+ in BC site is extracted from a frozen phonon calculation. Both thermal effects and the fact that our estimate is extracted by a situation in which the proton is visiting sites other than BC (e.g. the M site), can explain this discrepancy.

Since there are these remarkable differences in the vibrational spectra for the two paths, we suggest that scattering experiments could distinguish between these two situations.

Diffusion coefficient and activation energy

From an analysis of the mean square displacement of H^+ at long time t, we can measure the diffusion coefficient by using the Einstein relation $\lim_{t\to\infty} \frac{< [r(t) - r(0)]^2 >}{6t} = D$. In Fig. 3.1 we show the calculated value for D at three different temperatures (full circles), one of which corre-

sponds to an overheated crystal ($T \simeq 1950$). In the same figure are reported various experimental data that we have previously discussed. The agreement of the simulation with the experimental data of Van Wieringen and Warmoltz at high temperature is remarkable, considering that theory does not take into account presence of defects, possible molecular formation or other factors that could hinder the diffusion process. At T $\simeq$ 1200 K we obtain a diffusion coefficient D of the order of 10^{-4}cm^2/sec, thus confirming the high mobility observed in the experiment of ref. [62].

The average in the square displacement has been obtained by dividing the whole trajectory into different segments: For each of them one new initial configuration $r(0)$ is considered from which the square displacement is computed and then the average is taken over all the segments. The error bar, also shown in the picture, has been estimated by the variation of the coefficient D calculated in different segments of the trajectory.

From the slope of a linear fit to the three data points in Fig. 3.1 we obtain an activation energy $E_A = 0.33 \pm 0.25$ eV. Within this rather large error bar, this value is in reasonable agreement with 0.48 eV obtained from the only existing experimental data [62] in the same temperature range. It has to be noted that, due to the complexity of the H^+ diffusive motion illustrated above, it does not seem correct to identify E_A with a single energy barrier. It seems more adequate to consider E_A as an average barrier seen by the diffusing proton along its path.

3.2.4 Discussion and open questions

In conclusion, by using ab-initio MD simulations, we have studied the diffusion of a proton in c-Si at high temperatures.

This work demonstrates that dynamical effects substantially modify

the picture emerging from T=0 results. In particular we observed that the proton follows diffusive paths different from that expected from the study of the energy surface at T=0, and, as a consequence, sees a higher activation energy. We have detected two different diffusive paths in which the proton exhibits a very different vibrational density of states. Therefore we suggest that scattering experiments can help to establish the nature of the diffusive path.

Our results for the diffusion coefficient agree well with experiments in the studied range of temperatures, and confirm the high mobility of the proton in c-Si. We have found that the diffusion coefficient computed in the two different paths is the same within the error bar.

As we have mentioned before, possible quantum effects on the ionic motion (in particular on the light proton) are not considered in this study. Also for this reason we considered only the high temperature regime where we suppose these effects to be negligible. However, if we consider the value of the ratio $\hbar\omega/K_BT$ as an indicator of the importance of quantum effects on the dynamics, we cannot state that these are completely absent even for these high T. In fact the highest frequencies computed for the proton are around 0.2 eV, a value that is comparable with the thermal energy that comes into play. The study of quantum effects is a difficult one and outside the scope of our thesis. Quantum effects on H diffusion in metals have been analyzed both theoretically [74] and with computer simulation [73]: these studies indicate that in a system like Nb quantum effects are not negligible up to temperature of $\approx 300\ K$.

A dynamical correlation between successive passages of the proton in BC sites seems to be present. Indeed we observed that once the proton visited a BC site, is quite likely that after some time (always of the same order, i.e. $\sim 0.35\ psec$) it visits another BC along the same chain

of bond. We are carrying on further investigations on this point for exploring the possibility of the existence of some memory in the lattice that assists this event.

Chapter 4

The structure of Hydrogenated Amorphous Silicon

4.1 Introduction

The interest in hydrogenated amorphous silicon (a-Si:H) has grown enormously during the last decade as a consequence of its dopability and concomitant technological applications [2]. The possibility of efficient doping in the amorphous phase was demonstrated by W.E. Spear and P.G. LeComber in 1975 [93,94] and led to the first a-Si *p-n* junction [95]. This development has removed one of the main limitations of amorphous semiconductors and opened up possibilities for the fabrication of thin-film electronic devices, including photovoltaic solar cells.

It was soon clear that the presence of H was essential in modifying the electric properties of the amorphous material: It is generally agreed that a-Si produced by sputtering or evaporation, without H, contains a large number of coordination defects as seen in electron spin resonance (ESR) experiments. Gap states associated with these defects may explain the insensitivity of a-Si to dopants. When H is added to the amorphous network the ESR signal is strongly reduced: this is appar-

ently a consequence of H bonding to these defects, inducing a strong reduction of the gap states density of the material.

The understanding of the local structure order is, of course, fundamental to a full comprehension of the electronic properties of this material.

In this chapter we present some recent results of a numerical simulation on an a-Si:H sample generated by ab-initio MD: we concentrate on the short range order and the vibrational properties of this material, making direct contact with experimental results.

4.2 Short-range order

The short-range order (SRO) can be defined as the local structural arrangement around a given atom. In particular, for the case of covalently bonded amorphous solids, the SRO about an atom of type i can be characterized by the coordination number N_j of atoms of each type j, in a shell of atoms at a distance R_{ij} from the origin atom, and by the angle θ_{jik} subtended by the first neighbours j and k at atom i. Within this definition, the distances governed by SRO are quite small, typically of the order $2 \div 3$Å.

Because of the finite size of the MD box used in the simulation, the longest correlation length that one can treat with is equal to half of the linear size of the box. With the box used in our simulation, the maximum range of correlation is ≈ 5.4Å. This is sufficient for a study of the SRO of this system; instead, an analysis of the medium- and long-range structural order is out of the present computer performances.

Before to present the results of the simulation we briefly describe some of the experimental investigations on the a-Si:H structure.

4.2.1 Experimental probes for SRO

The most commonly used technique to probe the structure of amorphous solids uses diffraction of X-rays, neutrons or occasionally electrons. A review of the results of investigations which have been carried out to determine the structure of a-Si:H, has been recently presented by Elliott [96].

Since a-Si:H is a binary system, three partial pair correlation functions (Si-Si, H-Si, H-H) are needed to describe the short-range structure. Furthermore, the experimental investigation of a-Si:H is complicated by the fact that the material is not expected to be homogeneous, because of the presence of gross structural defects such as voids, internal cracks, etc.

A diffraction experiment gives the so-called structure factor $S(Q)$ as a function of the scattering vector Q. The structure factor $S(Q)$, which is a function in reciprocal space, is related to pair distribution functions in real space by means of a Fourier transform. It should be noticed that the transformation of experimental data to real-space distribution function would require the knowledge of $S(Q)$ for all values of Q. In practice, data can only be measured up to a maximum cut-off value of scattering vector Q_{max}. The result of performing a straight Fourier transformation of such data is to cause a loss of resolution as well as to introduce spurious oscillations at small distances.

In order to obtain the partial pair functions, it is necessary to perform as many scattering experiments as there are distinct partial functions by varying the relative values of the scattering factors in some way: In the case of neutron scattering experiments, *isotopic substitution* is the ideal method. This method consists in substituting one isotope of a given element by another of the same element. In such a way the chemistry and the structure are preserved in this process, but the neutron scattering

length can vary dramatically. In this respect, hydrogen is particularly suitable, because of the very marked difference in scattering length for the two isotopes, H and D. Isotopic substitution neutron scattering experiments have been performed on sputtered a-Si:(H,D) [97,98,99], the results of which will be discussed together with the results of our simulation.

In X-ray and electron diffraction, the total scattering intensities are determined only by Si-Si pair correlations because H is essentially invisible; therefore the comparison with neutron scattering experiments can be made only for the Si-Si partial correlation function. X-ray diffraction data for sputtered a-Si:H have been presented in ref. [100].

Extended X-ray absorption fine structure (EXAFS) provides another direct structural probe, complementary to the diffraction technique, which also can yield partial pair distribution information. A number of EXAFS experiments have been carried out for both pure and hydrogenated amorphous silicon [101,102].

Another technique which can be used to determine the H-related configurations present in the sample, is the infrared spectroscopy. Lucovsky and Pollard in ref. [2] have reviewed the applications of this technique for structural study of a-Si:H. The reason why the infrared spectroscopy is useful for the study of a-Si:H is related to the very different ranges of frequencies corresponding to modes involving silicon atoms ($0 < \omega < 550\ cm^{-1}$) and H in a-Si:H ($600 < \omega < 2100\ cm^{-1}$). The H-related frequencies occur at a considerably higher regime due to the light mass of H. Therefore H-related modes can be identified unambiguously from infrared absorption spectra. Infrared spectra for samples of a-Si:H was obtained by Lucovsky et al. [91]. From a comparison of infrared mode frequencies found in various types of Si-H groups, it has been possible to assign peak positions in the infrared spectrum to each

of the possible structural groupings [2], namely monohydride (Si-H), dihydride ($Si-H_2$) or even "polysilane" groupings $(Si-H_2)_n$.

Inelastic neutron scattering experiments have been also performed for the study of the vibrational density of states (VDOS) on pure a-Si [103,104] and a-Si:H [103]. It should be noted that inelastic neutron scattering experiments on a-Si:H yield essentially only the partial VDOS for H-related vibrations, because hydrogen has a very large and primarily incoherent neutron scattering cross-section. Therefore the Si-related VDOS can only be obtained from samples of pure a-Si.

Finally a particularly fruitful source of information is given by nuclear magnetic resonance (NMR) of hydrogen in a-Si:H samples [105].

4.3 Computer generation of an a-Si:H sample

We considered a SC supercell containing 64 silicon atoms initially arranged in the perfect crystalline positions, and 8 neutral hydrogen (H^0) atoms located in different interstitial (Td) sites of the lattice. This corresponds to about 11% at. H concentration (real material that exhibits useful electronic properties contains hydrogen in the $\approx 2 \div 16$ atomic percent range). The volume of the box is fixed at the experimental value of c-Si.

The plane waves expansion of the wavefunctions has been truncated at a G_{max} corresponding to $12\,Ry$; for the expansion of the potentials we used a value of $\sqrt{2}G_{max}$ (we have verified that the change in the total energy is negligible if we instead consider the appropriate value $2G_{max}$). The Γ point has been used for the BZ sampling. We adopted the same pseudopotential as described in the previous chapter for the study of H in c-Si. We set, again as in the previous study, the fictitious mass $\mu = 200 a.u.$ and the time step $\Delta t = 1.21 \times 10^{-16} sec.$

We heated the system up to a temperature of about $2200K$ for which it has reached the liquid phase. We let the liquid evolve for more than $1psec$: the Si-Si pair correlation function $g_{Si-Si}(r)$ calculated in this time interval, exhibits a coordination number $N \approx 6$, which agrees with the experimental value for liquid Silicon. Starting from this equilibrated liquid structure, we quenched the system to $300K$. The cooling rate was in average around $5. \times 10^{14} K/sec$: however we lowered this rate by a factor of two when the system was approaching the non-diffusive regime ($\approx 1000K$). This thermal treatment has been performed by the use of constant temperature-constant volume MD, as described in section 1.3.2, and periodically quenching the electronic coordinates: this was necessary because, expecially for the highest temperatures, the electrons acquire rapidly classical kinetic energy from the ions. Instead, when the amorphous phase is reached, this is no more the case, and we adopted the usual equations of motion appropriate for microcanonical MD simulations and no further minimization was necessary: The transfer of energy from the ionic to the electronic degrees of freedom was negligible during the whole run at $T = 300K$.

The structure generated in this way has been equilibrated for about 1.5 *psec* and statistical averages have been taken over this time interval.

After this an additional annealing cycle was performed in which the temperature of the sample was first raised up to $\approx 1100K$. At this temperature the system underwent strong relaxations. Afterwards we quenched again the system to $300K$ with the same cooling rate as before. The entire annealing cycle took about 3 *psec*. The new amorphous structure obtained in this way has been finally equilibrated for ≈ 2 *psec*.

We will discuss in the next section the structure of the a-Si:H thus generated and will describe the differences between the sample *before* and *after* annealing. A direct comparison with experiment will be also

shown.

4.4 SRO of simulated sample

The first evident effect of the annealing cycle is that the internal energy of the amorphous structure after annealing is about 34 $meV/atom$ lower than before annealing, showing that relevant relaxations occurred during the process. An analysis of the partial pair correlation functions (PPCF) will elucidate what kind of structural modification occurred in the sample. In fig. 4.1 we show the three PPCF's *before* and *after* annealing at a temperature of about $300K$. The average is taken over all the configurations during the MD run, i.e. during about 1.5 *psec*. No smoothing procedure has been performed on the simulation data.

4.4.1 The Si-Si distribution function

The Si-Si PPCF in fig. 4.1 reflects the local tetrahedral order characteristic of the material. It exhibits a very well defined first peak at a distance $r_1 \simeq 2.35$ Å, with a coordination number $N_1 \simeq 3.9$, that is slightly smaller than the value 4 expected for a perfect tetrahedral network, as also found in experiment [97]. A second much broader peak occurs at $r_2 \simeq 3.80$ Å.

The agreement with the experimental $g_{Si-Si}(r)$ obtained by Menelle [99] is excellent as can be seen in fig.4.2 where we reported the $g_{Si-Si}(r)$ after annealing. The experimental values are those before filtration: the spurious oscillations at small distances are an effect of the Fourier transformation as discussed in paragraph 4.2.1.

The effect of the annealing cycle is small but appreciable. Both the first and the second peak become higher and a small displacement of r_2 is observed. This results in an overall better agreement with experiment.

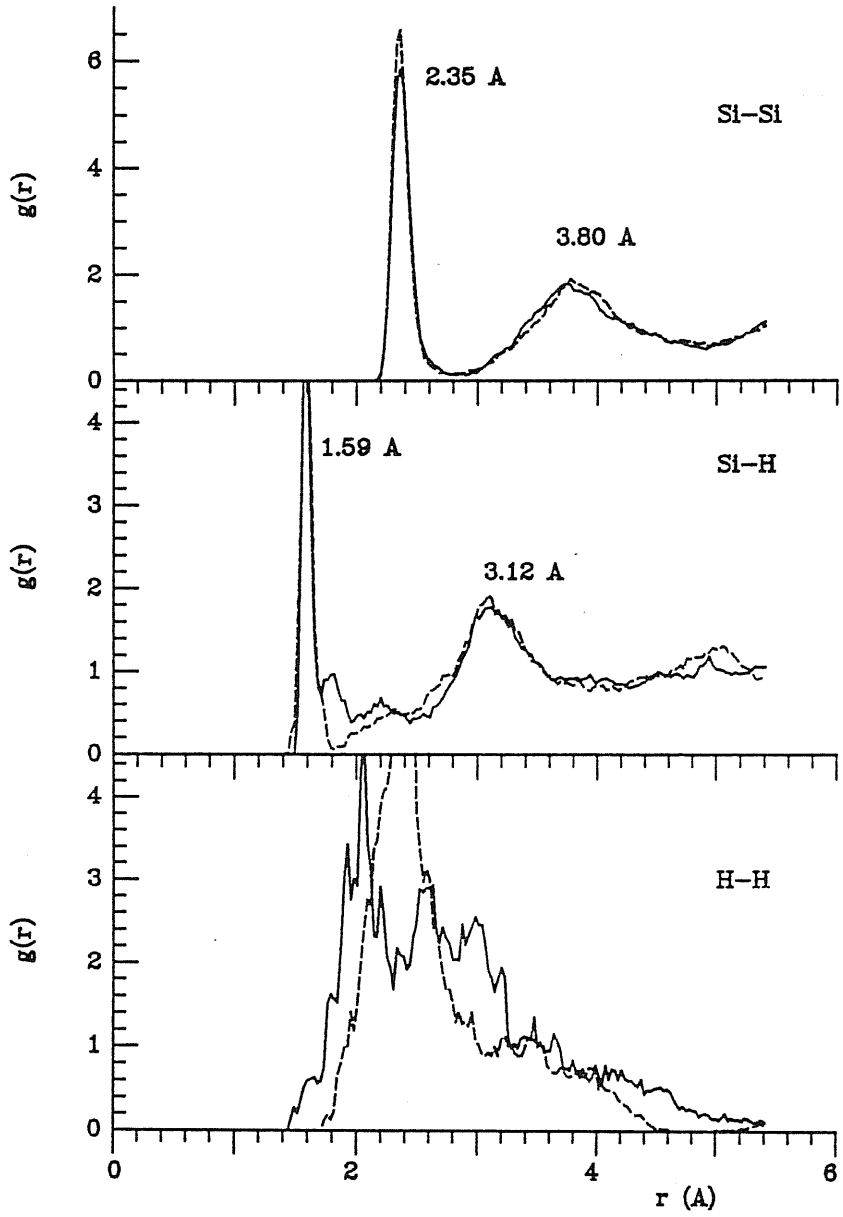

Figure 4.1:
Calculated Partial Pair Correlation Functions in a-Si:H before annealing (full lines), after annealing (Dashed lines). The numbers indicate the position of the peaks after annealing.

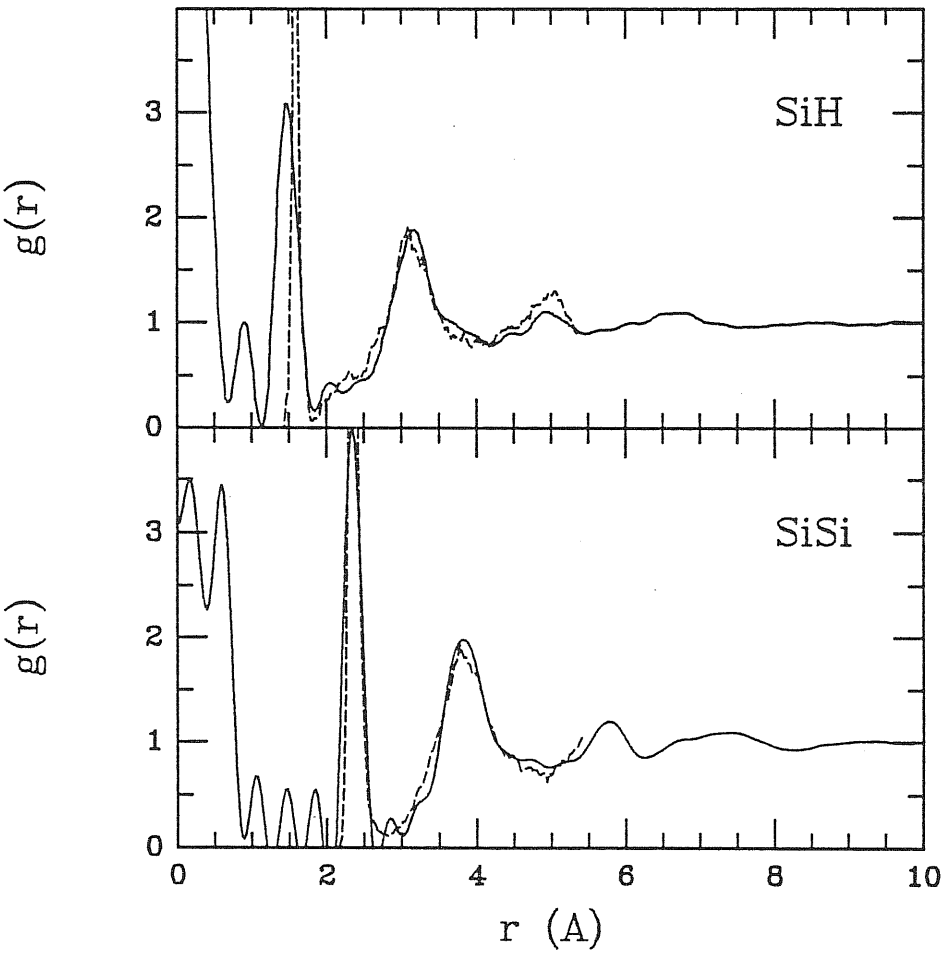

Figure 4.2:
Partial Pair Corrrelation Functions in a-Si:H. Full lines: Experimental data from ref. [99]. Dashed lines: Present calculation after annealing. The H-H function is not reported because of the large noise present both in the experiment and in the simulation.

4.4.2 The Si-H distribution function

Two well defined correlations are present in the Si-H PPCF in fig. 4.1: the sharp first peak occurs at $r_1 \simeq 1.59$ Å and the second at $r_2 \simeq 3.12$ Å. The first peak is related to Si-H groups with a well defined bond length: in almost all the cases the silicon atom in these monohydrides is bonded to other 3 silicon atoms, confirming that H saturates dangling bonds. The effect of the annealing cycle is quite evident in this correlation function: some small structures, between the first and the second peak, are present *before* annealing, but disappear in the annealed sample. In particular, the shoulder after the first peak is related to configurations in which H (2 cases out of 8) is located in "quasi-interstitial" sites between two silicon atoms: the weak bond lengths in these Si-H-Si configurations are around 1.8 Å and H is not necessarily located symmetrically by respect to the two Si atoms. In both cases that are present in our sample *before* annealing, the two nearest Si atoms are, by respect to the surrounding silicon ions, one threefold-coordinated (T_3), and the other fourfold-coordinated (T_4). (A similar configuration has been studied in the theoretical work of ref. [106]). The existence of these Si-H-Si three-center bonds has been first proposed by Fish and Licciardello [107]. In ref. [108] an H-interstitial mechanism is postulated to explain the measured stress. The relaxation of these weakly bonded hydrogen (WBH) configurations in more stable tightly bonded (TBH) monohydrides with the annealing, is consistent with the picture of an exodiffusion study in ref. [109]. At present, the dynamics of these relaxations in connection with the diffusion of H in a-Si:H is object of further investigations.

After annealing all the H atoms are bonded to a single Si atoms: this situation is clearly evidenced by the coordination number N_1 which is exactly 1. In 7 cases out of 8 the Si atom near H is bonded to 3 other Si atoms; in the remaining case the Si atom is fourfold-coordinated. No

dihydride grouping is present in the sample, confirming the conclusion of experimental results [99] for which the occurrence of (Si-H_2) configurations, with this concentration of H atoms, is quite rare.

In fig.4.2 we show the computed $g_{Si-H}(r)$ after annealing, together with the experimental neutron scattering data [99]. Again spurious oscillations for small values of r are present in the experimental data. The agreement is very good also for this PPCF. The position of the first peak is slightly larger than the experimental one: in fact this is about the same error we have in the computation of the bond length in the SiH molecule (see Tab. 3.1).

4.4.3 The H-H distribution function

The information obtainable by experimental H-H partial distribution function is less reliable in view of the large uncertainties in the extraction of the H-H structure factor. However there is an indication of a broad peak in the H-H PPCF lying in the range $2.2 \div 2.6$ Å. This peak was interpreted as an indication of the presence of dihydride units [97]. However in the recent neutron scattering study of ref. [99], on a sample with 12% concentration of H atoms, it has been shown that the presence of this broad peak can be also explained without resort to dihydride units.

In fig. 4.1 we show the computed H-H PPCF *before* and *after* the annealing treatment: this function gives a clear evidence for H clustering, strongly enhanced in the annealed sample. A broad peak centered at ≈ 2.4 Å is recovered in good agreement with the experimental one. Because of the absence of dihydride units in our sample, we support the suggestion that this peak can be explained with the presence of only Si-H groups.

We analyzed in detail the cluster configurations evidenced in the

pair distribution function: Two small clusters containing 4 H atoms each are present. In one of these, the 4 H atoms occupy the edges of a distorted square in a quasi-planar configuration; in the other cluster, 3 H atoms form a triangle with similar side lengths and the fourth lies on the extension of one side of the triangle. Recent multiple-quantum NMR studies [110] have suggested the existence of clustering effects, with a predominant bonding environment of 4 to 7 atoms. Our results, although limited by finite size effects, strongly support the validity of this picture.

At present, we have not characterized precisely what kind of interactions are present between H atoms. However we noted that some of the features of H clustering are very similar to those characterizing defect clustering in pure a-Si [111]. Therefore we suggest that the clustering effect in the H-H PPCF is not due to direct H-H interaction, but is rather an effect mediated by the underlying disordered network.

4.5 Coordination defects and bond angle distribution

An interesting analysis of the local order in the silicon network is gained looking at the first coordination number N_1 of the individual atoms and its time evolution during the run.

It was generally believed that the dominant paramagnetic center (D-center) in a-Si is the dangling bond (threefold-coordinated Si atoms) and that the density of these centers is reduced by H through the formation of Si-H bonds. Recently Pantelides [112,113] proposed that overcoordination occurs in a-Si and that threefold- (T_3) and fivefold-coordinated Si atoms (T_5: floating bonds) are the primitive intrinsic defects. This suggestion has been confirmed by both conventional MD [114] and ab-initio MD simulations on a-Si [26,115,111] in which both T_3 and T_5 defects are

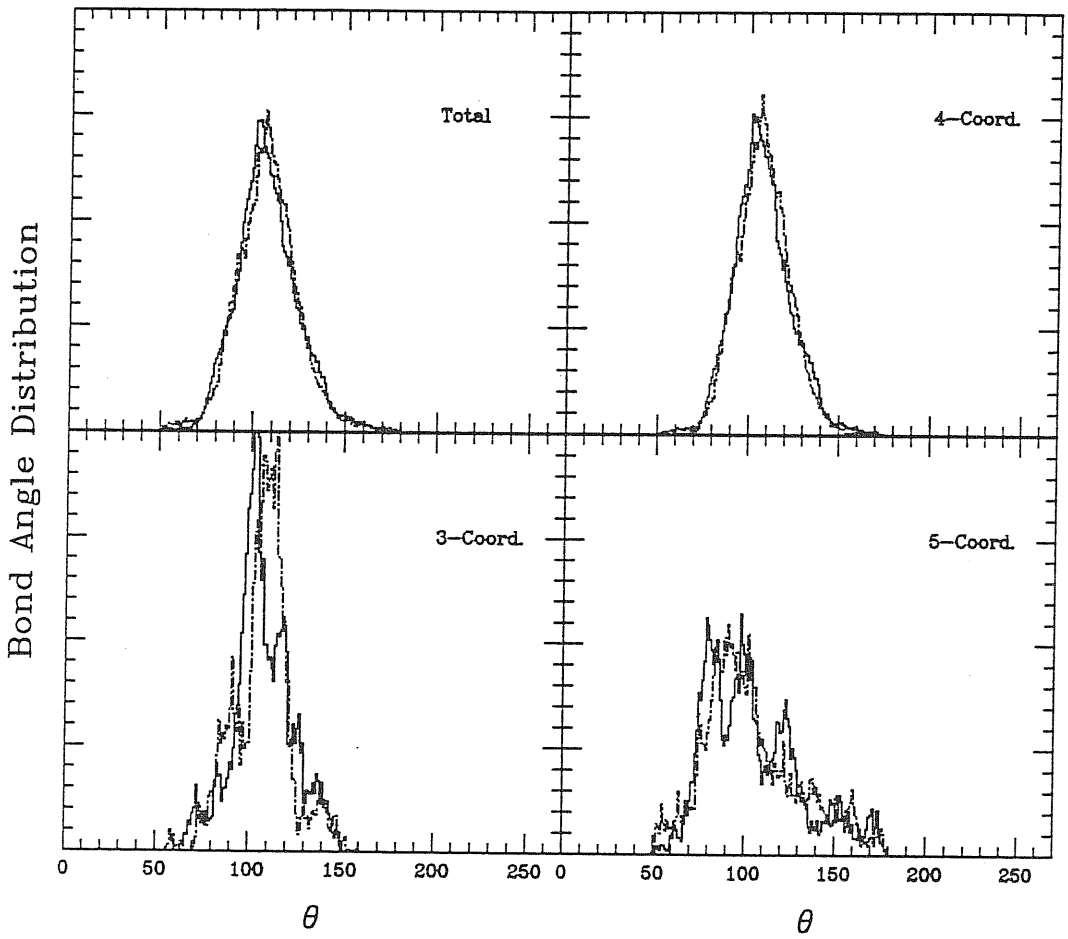

Figure 4.3:
Bond Angle Distribution (see text) for the simulated a-Si:H. Full lines: Before the annealing. Dash-dotted lines: after the annealing.

found with comparable formation energies: these two defects may be converted into one another via network distortion. Therefore both of these defects present in the amorphous structure are better characterized as *weak* bonds. However it is not clear if some of these defects can be related to the D-centers seen in real a-Si. Very recently [116] the hyperfine splittings of these defects was calculated and compared to experiments.

In the a-Si:H sample we find again both T_3 and T_5 defects with a predominance of T_3. The number of these defects is not significantly changed after the annealing. We find that the threefold-coordinated silicon atoms that do not change the coordination during the whole run, are all bonded with an H atom. The remaining defects are predominantly T_5 but fluctuate during the simulation. For the T_5 atoms we observe that usually two or three bond lengths are longer compared with r_1 in the $g_{Si-Si}(r)$.

Another information about SRO comes from the bond angle distribution (BAD), where the angle θ_{jik} has been defined above. In fig. 4.3 we report the BAD of the sample *before* and *after* annealing averaged over the entire run. In the different insets we show the total BAD and that calculated separately for the three-, four-, and five-coordinated atoms. The recovering of the tetrahedral network is demonstrated by the very sharp peak around an angle slightly less than tetrahedral ($\theta \simeq 109°$). The annealing makes the BAD more peaked and the position of the peak becomes nearer to the tetrahedral angle, demonstrating that the annealed structure is more ordered. The average value is $\theta \simeq 107.5°$ and the standard angular deviation $\sigma \simeq 16.5°$. This value should be compared with the experimental estimate in the range $7 \div 10°$ [117]. Our overestimate is possibly due to the high concentration of coordination defects present in the simulated sample by respect to the real one, as

well as to finite size effects. Furthermore, the experimental value of σ is extracted in a very indirect way. In an ab-initio MD study for a-Si [111], a better agreement was found, calculating σ via an analysis similar to that performed in experimental works.

4.6 Vibrational properties

The computation of the velocity-velocity correlation function Z(t) in MD simulations allows for an analysis of the vibrational properties of the system. Indeed the Fourier spectrum of the Z(t) gives the VDOS. In numerical simulation it is clearly possible to compute separately the contributions at the VDOS relative to different components in the system. We discuss first the Si-related vibrational properties and then those related to H.

4.6.1 Si-related VDOS

As we discussed in section 4.2.1, inelastic neutron scattering experiments can detect the Si-related vibrational states only on pure a-Si. The $Z(\omega)$ for a-Si displays four features that correspond to the four major peaks in the phonon density of state for c-Si at $20, 40, 50$ and 60meV that are conventionally referred to as TA, LA, LO, and TO peaks [103,104]. Ab-initio MD simulations on pure a-Si [26,115,111] reproduce with accuracy the experimental VDOS, as shown in fig 4.4.

The calculated Si-related VDOS for the a-Si:H sample after annealing at $T \simeq 300\ K$ is given in fig. 4.5. We note that the all four features present in the experimental VDOS for pure a-Si are also visible in this picture. The main difference is that the intensity of the TO peak is much lower in the hydrogenated sample than in pure a-Si. This can be an effect induced by the presence of H that substantially modifies the force constants in the Silicon atoms involved in the monohydride groups.

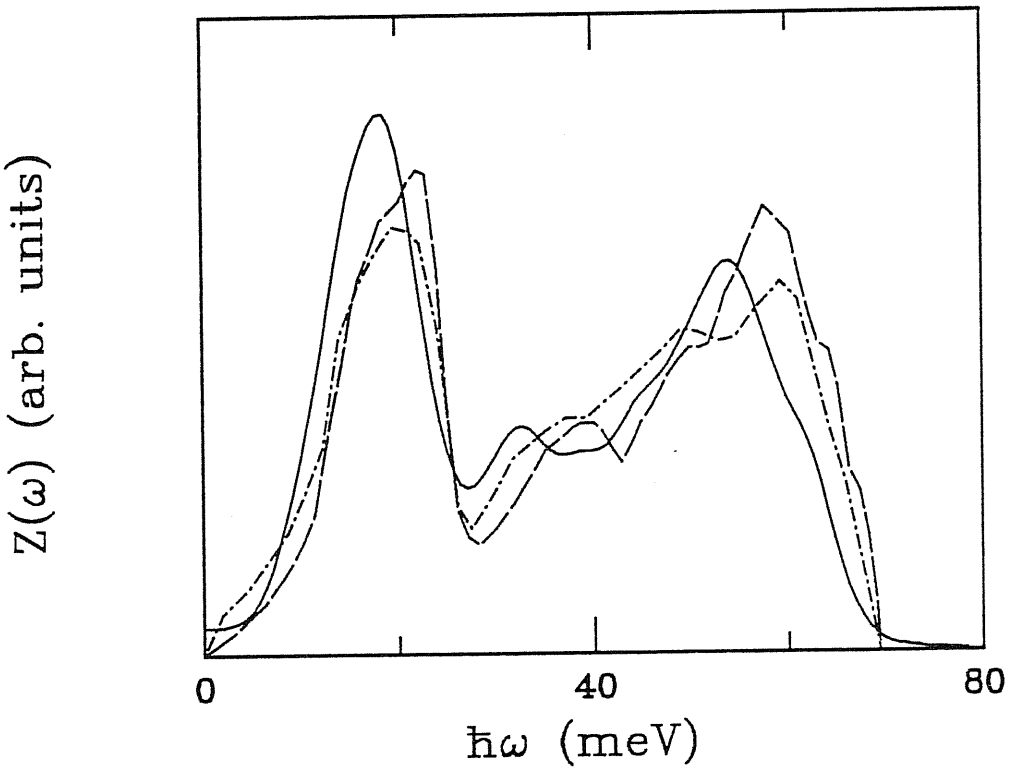

Figure 4.4:
Vibrational Density of States in a-Si. Full line: Ab-initio Molecular Dynamics simulation [111]. Dashed line: Experimental data from ref [104]. Dash-dotted line: Experimental data from ref [103].

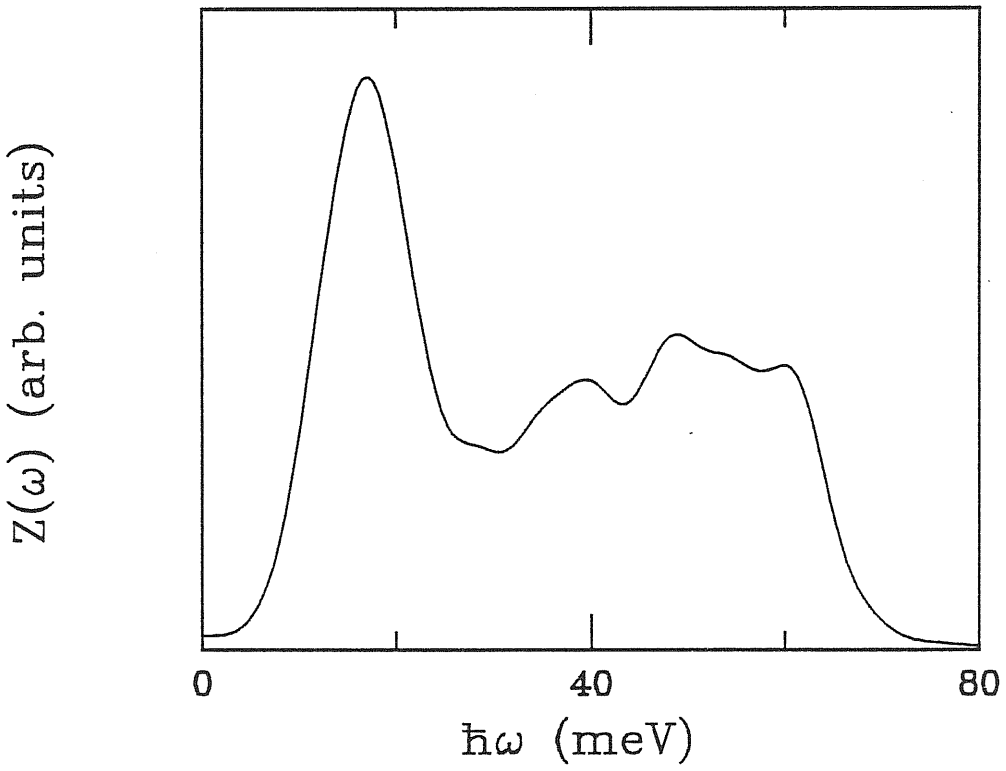

Figure 4.5:
Calculated Silicon-related Vibrational Density of States in a-Si:H.

Indeed we have verified that if we calculate the VDOS by selecting the silicon atoms that are not involved directly in the Si-H bonds, the resulting TO peak is more enhanced. Unfortunately, as mentioned before, the $Z_{Si-Si}(\omega)$ in a-Si:H cannot be measured directly with neutron scattering. However, far-infrared absorption spectra of pure and hydrogenated a-Si with different H concentrations [118] show a reduction of the intensity in the TO peak with increasing H percentage, consistent with our findings.

4.6.2 H-related VDOS

H-related frequencies in a-Si:H have been extensively studied by infrared spectroscopy [119]. The results of ref. [91] are reported in fig. 4.6. The infrared bands around 630 cm^{-1} and 2000 cm^{-1} have been unambiguously identified as the bond-bending mode and the stretching mode of monohydride groupings, respectively. The band around 900 cm^{-1} has been assigned to the scissor bending mode of ($Si-H_2$) units. we give the H-related VDOS calculated before and after annealing of the a-Si:H sample. Both the bending and the stretching modes of the Si-H units present in the generated structures, are well defined. We underestimate the frequency of the stretching band of about 10% (this is the same error we have in the calculation of the frequency for the Si-H molecule: see Tab. 3.1). The bending mode frequency is about 5% lower than the experimental value.

The effect of the relaxation of the WBH configurations in TBH with the annealing is visible in the H-related VDOS: A small peak around 1100 cm^{-1} related to vibrational modes of these WBH units, disappears in the annealed sample. Furthermore the intensity of the stretching band is strongly enhanced after annealing. The absence of ($Si-H_2$) units in our sample has as counterpart in the VDOS, the absence of the band

around 900 cm^{-1}. We noticed that the spread in the stretching band is related with the spread in the bond length of the Si-H units. In particular we found that there is a linear relation between the bond lengths and the value of the stretching frequency. It is plausible that if performing a further annealing procedure the tails of the stretching band further reduce.

In fig. 4.7 As far as the frequency range $0 < \omega < 550\ cm^{-1}$ is concerned, inelastic neutron scattering experiments [103] showed that the H-related VDOS exhibits, besides resonant modes with the Si-related frequencies, a small peak at 27 meV = 215 cm^{-1} that is not present in the Si-related VDOS. Because of the small number of H atoms in our sample the signal of the calculated H-related VDOS in this range of frequency has a strong noise making difficult a precise assignment of the different structures. However the peak at 27 meV seems to be present in our data and is the object of further investigations.

4.7 Conclusions and discussion

In conclusion we have studied the short range order of an hydrogenated amorphous silicon structure generated by a computer simulation in which the only input experimental parameters are the ionic masses. The density of the simulated sample has been fixed to the value of the c-Si according to recent experimental results [99] and the concentration of H atoms is about 11%.

The agreement of the calculated partial pair correlation functions with those obtained experimentally by neutron scattering experiments is overall very good. The tetrahedral order of the amorphous silicon network is preserved by the introduction of hydrogen.

H is preferentially bonded to a single Si atom which is characterized as a T_3 defect. Our results indicate that (Si-H_2) units, with the present

H concentration, are not likely.

The H-H partial correlation function exhibits an interesting clustering effect that is tentatively related to a tendency of the coordination defects in the silicon network to cluster. A more detailed analysis of this point is in process.

An annealing treatment of our sample has shown the presence of weak bonded hydrogen units that relax in more stable monohydrides groups. This observation constitutes a good starting point for a study of the diffusion process of H within the a-Si network that is currently under way.

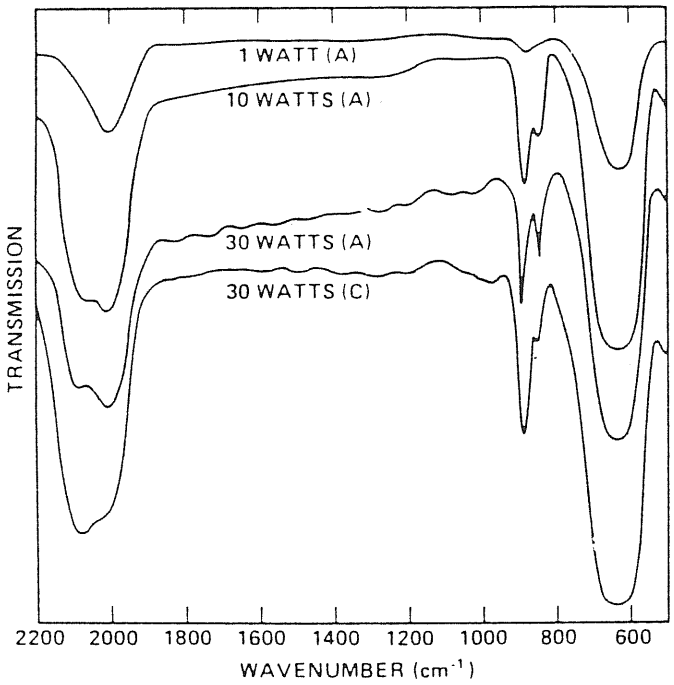

Figure 4.6:
Infrared Trasmission Spectra for glow-discharge in a-Si:H, deposited on Anode (A), deposited on Cathod (C) [91]

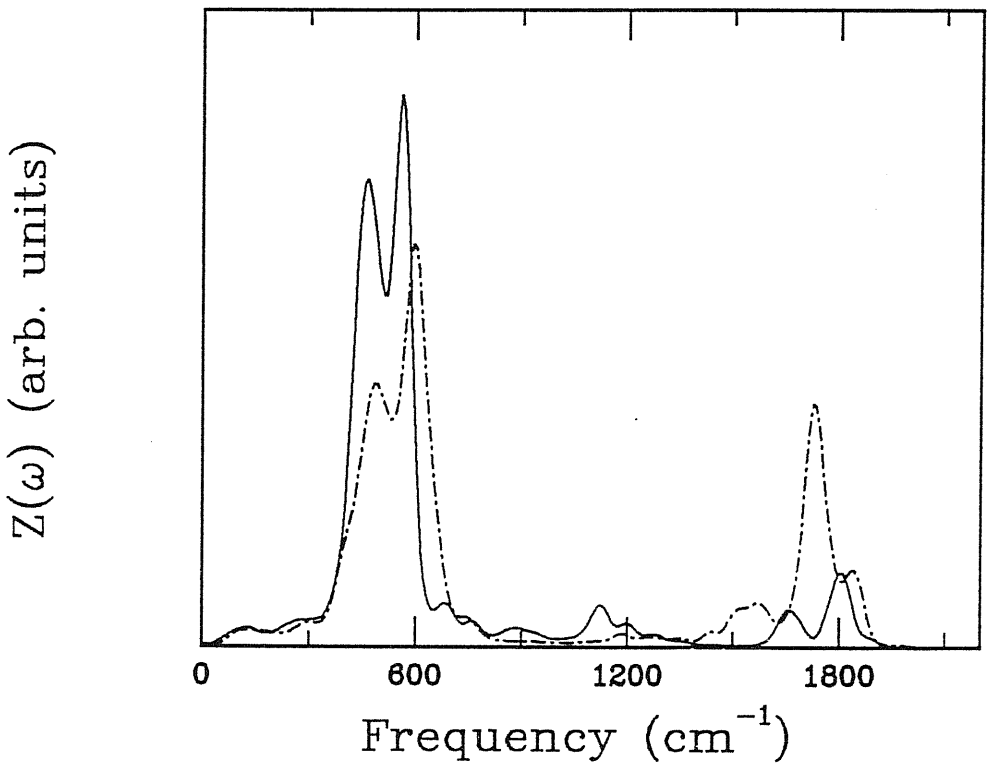

Figure 4.7:
Calculated Hydrogen-related Vibrational Density of States in a-Si:H. Full lines: Before the annealing. Dash-dotted lines: after the annealing.

Chapter 5

Conclusions

In this work we have analyzed the microscopic behaviour of Hydrogen both in crystalline and amorphous Silicon.

For this purpose we have used the ab-initio Molecular Dynamics method. This approach allows to perform computer simulations of semiconducting and metallic systems at finite temperature. We have stressed that in ab-initio Molecular Dynamics, the interatomic potential is obtained with the same accuracy of "standard" Local Density Functional calculations.

For the first time dynamical effects have been included explicitly in the simulation of a diffusive proton in the c-Si lattice. Due to dynamical effects the behaviour of the proton is substantially different from that inferred from static total energy calculations. The diffusion coefficient calculated from the simulation and its temperature dependence is in very good agreement with the available experimental data. This confirms the high mobility of H in c-Si. An analysis of the Hydrogen-related vibrational properties suggested that scattering experiments may distinguish between different diffusion mechanisms.

Finally we presented some recent results on a computer generated hydrogenated amorphous sample. In particular we have described in detail the short range order and the vibrational properties exhibited by

the simulated a-Si:H sample. The agreement with available experimental results is very good both for structural and dynamical quantities. In our sample Hydrogen is bonded to Si ions only in a monohydride form. This confirms the tendency of H to saturate the dangling bonds present in amorphous Silicon samples.

Appendix A

Cut-off parameters

The sum over G in the expansion of the wavefunction (eq. (1.12)) is usually truncated to include only M plane waves up to a cutoff G_{max} corresponding to an energy cut-off $Ecut$. As a consequence of eq. (1.1), the electronic density is then expanded in many more plane waves, namely all that corresponding to vectors G′ that are difference vectors of wavevectors (k + G) in expansion (1.12). Therefore, the electronic density, and the potentials, should be expanded up to $2G_{max}$ (i.e. up to a cutoff $4 \times Ecut$). Often the use of this high cutoff for the potential is unnecessary [120,121]: it is possible introduce a smaller cut-off for the potential without considerably reduce the accuracy of the final results. The most drastic choice is to assume the same cutoff for wavefunctions and potentials (${G_{max}}^{\psi} = {G_{max}}^{V}$) The saving in computer time and storage space can be very relevant expecially for large systems. However some care must be taken when using this approximation: it is clear that when increasing G_{max} the results will converge at the same value; but if the number of plane waves is far from the convergence, the results can be not only quantitatively different but also qualitatively wrong. This depends strongly on the system and therefore tests are necessary to assess the goodness of this approximation.

Appendix B

The Verlet algorithm

The problem is to convert the differential equations of motion into a set of difference equations which enables us to go from time t to $t+\Delta t$ with a suitable chosen Δt. The simplest algorithm that we can use is the Verlet algorithm [28]. Let us consider the generic dynamical degree of freedom of the system $q(t)$; we have:

$$q(t+\Delta t) = q(t) + \Delta t\dot{q}(t) + \frac{1}{2}(\Delta t)^2\ddot{q}(t) + \dots \tag{B.1}$$

$$q(t-\Delta t) = q(t) - \Delta t\dot{q}(t) + \frac{1}{2}(\Delta t)^2\ddot{q}(t) - \dots \tag{B.2}$$

therefore we obtain

$$q(t+\Delta t) = 2q(t) - q(t-\Delta t) + (\Delta t)^2\ddot{q}(t) + O(\Delta t^4) \tag{B.3}$$

If m is the mass and V the interatomic potential, the acceleration of the coordinate $q(t)$ is given by

$$\ddot{q}(t) = \frac{1}{m}\left(-\frac{\partial V}{\partial q}\right) \tag{B.4}$$

Therefore the only information that needs to be carried in memory is $q(t-\Delta t)$ and $q(t)$. Using all the $q(t)$ we first calculate the forces and then all the $q(t+\Delta t)$ from eq. (B.3).

It will be noticed that the new coordinates $q(t + \Delta t)$ have been obtained without reference to the velocities at time t. These can be obtained by taking the difference between eq. (B.1) and eq. (B.2):

$$\dot{q}(t) = \frac{q(t + \Delta t) - q(t - \Delta t)}{2\Delta t} + O(\Delta t^3) \tag{B.5}$$

and then we can calculate the kinetic energy at that time.

Acknowledgments

I would like to express my gratitude to Roberto Car and Michele Parrinello for their constant help and support throughout the period I spent at SISSA.

Most of the results presented in this thesis have been obtained in collaboration with my friend Guido Chiarotti. I wish to thank Guido for his critical reading of several parts of the manuscript and for his help in the final version of this thesis.

I thank Furio Ercolessi, Giorgio Pastore, Enrico Smargiassi and Ivan Stich for many stimulating discussions that contributed to this work.

I am indebted with A. Menelle for providing us recent experimental data on a-Si:H.

I am grateful to Giulia for her constant support.

The computations presented in this thesis were carried out under the SISSA-CINECA (Centro di Calcolo Elettronico dell'Italia Nord-Orientale) collaborative project, sponsored by the Italian Ministry for Public Education.

Bibliography

[1] See, for instance, S. J. Pearton, J. W. Corbett and T. S. Shi, *Appl. Phys. A* **43**, 153 (1987)

[2] See, for instance, *The Physics of Hydrogenated Amorphous Silicon*, edited by J. D. Joannopulos and G. Lucovsky, Springer-Verlag, 1984

[3] P. Hohenberg and W. Kohn, *Phys. Rev.* **136**, B864 (1964)

[4] W. Kohn and L. J. Sham, *Phys. Rev.* **140**, A1133 (1965)

[5] See for instance the recent review, R. O. Jones and O. Gunnarsson, *Rev. Mod. Phys.* **61**, 689 (1989)

[6] See the review article by Chris Van de Walle in the book *Hydrogen in Semiconductors*, to appear

[7] R. Car and M. Parrinello, *Phys. Rev. Lett.* **55**, 2471 (1985)

[8] For a recent overview see *Molecular-Dynamics Simulation of Statistical-Mechanical Systems*, edited by G. Ciccotti and W.G. Hoover (North-Holland, Amsterdam, 1986)

[9] F. H. Stillinger and T. A. Weber, *Phys. Rev. B* **31**, 5262 (1985)

[10] R. Biswas and D. R. Hamann, *Phys. Rev. Lett.* **55**, 2001 (1985)

[11] J. Tersoff, *Phys. Rev. Lett.* **56**, 632 (1986)

[12] See, for instance, the review article in *Theory of the Inhomogeneous Electron Gas*, S. Lundqvist and N. H. March, (Plenum, New York, 1983)

[13] See for instance Marvin L. Cohen, *Ann. Rev. Mater. Sci.* **14**, 119 (1984) and references therein

[14] D.R. Hamann, M. Schlüter and C. Chiang, *Phys. Rev. Lett.* **43**, 1494 (1979)

[15] G.B. Bachelet, D.R. Hamann and M. Schlüter, *Phys. Rev. B* **26**, 4199 (1982)

[16] S. Kirkpatrick, G. D. Gelatt, Jr. and M. P. Vecchi, *Science* **220**, 671 (1983)

[17] R. Car, M. Parrinello and W. Andreoni, in *Microclusters*, edited by S. Sugano, Y. Nishina, and S. Ohnishi, Springer-Verlag, Berlin, pag.134 (1987)

[18] P. Ballone, W. Andreoni, R. Car and M. Parrinello, *Phys. Rev. Lett.* **60**, 271 (1988)

[19] P. Ballone, W. Andreoni, R. Car and M. Parrinello, *Europhys. Lett.* **8**, 73 (1989)

[20] D. Hohl, R. O. Jones, R. Car and M. Parrinello, *Chem. Phys. Lett.* **139**, 540 (1987)

[21] D. Hohl, R. O. Jones, R. Car and M. Parrinello, *J. Chem. Phys.* **89**, 6823 (1988)

[22] D. Hohl, R. O. Jones, R. Car and M. Parrinello, *J. Am. Chem. Soc.* **111**, 825 (1989)

[23] I. Stich, R. Car, M. Parrinello and S. Baroni, *Phys. Rev. B* **39**, 4997 (1989)

[24] J. P. Ryckaert, G. Ciccotti and H. J. C. Berendsen, *J. Comp. Phys.* **23**, 327 (1977)

[25] F. Buda, R. Car and M. Parrinello, *Phys. Rev. B* , to appear

[26] R. Car and M. Parrinello, *Phys. Rev. Lett.* **60**, 204 (1988)

[27] Giulia Galli, Richard M. Martin, R. Car and M. Parrinello, *Phys. Rev. Lett.* **62**, 555 (1989)

[28] L. Verlet, *Phys. Rev.* **159**, 98 (1967)

[29] R. Car and M. Parrinello, in *Simple Molecular Systems at Very High Density*, edited by A. Polian, P. Loubeyre, and N. Boccara, Plenum, New York (1989), pag.455

[30] R. Car and M. Parrinello: Comment on: Error cancellation in the MD method for total energy calculations, *J. Phys.: Condensed Matter* , to appear

[31] Giulia Galli and R. M. Martin, private communication

[32] G. Pastore, E. Smargiassi and F. Buda, in preparation

[33] I. Stich, R. Car, M. Parrinello, Phys. Rev. Lett., to appear

[34] Giulia Galli, Richard M. Martin, R. Car and M. Parrinello, *Phys. Rev. Lett.* **63**, 988 (1989)

[35] S. Nosè, *Mol. Phys.* **52**, 255 (1984)

[36] S. Nosè, *J. Chem. Phys.* **81**, 511 (1984)

[37] A. Baldereschi, *Phys. Rev. B* **7**, 5212 (1973)

[38] D. J. Chadi and M. L. Cohen, *Phys. Rev. B* **8**, 5747 (1973)

[39] H. J. Monkhorst and J. D. Pack, *Phys. Rev. B* **13**, 5189 (1976)

[40] F. Buda, Magister Thesis, Trieste, 1986

[41] L. Kleinman and D.M. Bylander, *Phys. Rev. Lett.* **48**, 1425 (1982)

[42] H. C. Andersen, *J. Chem. Phys.* **72**, 2384 (1980)

[43] M. Parrinello and A. Rahman, *Phys. Rev. Lett.* **45**, 1196 (1980)

[44] M. Parrinello and A. Rahman, *J. Appl. Phys.* **52**, 7182 (1981)

[45] P. Gomes Dacosta, O. H. Nielsen, and K. Kunc, *J. Phys. C* **19**, 3163 (1986)

[46] O. H. Nielsen and Richard M. Martin, *Phys. Rev. Lett.* **50**, 697 (1983)

[47] O. H. Nielsen and Richard M. Martin, *Phys. Rev. B* **32**, 3780 (1985)

[48] O. H. Nielsen and Richard M. Martin, *Phys. Rev. B* **32**, 3792 (1985)

[49] W. Andreoni, G. Pastore, R. Car, M. Parrinello, and P. Giannozzi, in *Band Structure Engineering in Semiconductor Microstructures*, edited by R. A. Abram and M. Jaros, Plenum, (1989)

[50] J. Q. Broughton and P. B. Allen, in *Proc. of MRS Symp.*, edited by J. Broughton, W. Krakow, and S. T. Pantelides, 1986, Vol. 63

[51] J. Q. Broughton and X. P. Li, *Phys. Rev. B* **35**, 9120 (1987)

[52] Landolt-Börnstein, *Crystal and Solid State Physics*, Springer-Verlag, Berlin (1982), Vol. 17a

[53] B. Bech Nielsen, J. U. Andersen and S. J. Pearton, *Phys. Rev. Lett.* **60**, 321 (1988)

[54] S. J. Pearton and A. J. Tavendale, *Phys. Rev. B* **26**, 7105 (1982)

[55] J. I. Pankove, D. E. Carlson, J. E. Berkeyheiser and R. O. Wance, *Phys. Rev. Lett.* **51**, 2224 (1983)

[56] S. J. Pearton, *J. Electron. Mater.* **14a**, 737 (1985)

[57] N. M. Johnson, *Appl. Phys. Lett.* **47**, 874 (1985)

[58] N. M. Johnson, C. Herring, and D. J. Chadi, *Phys. Rev. Lett.* **56**, 769 (1986)

[59] C. H. Seager and R. A. Anderson, *Appl. Phys. Lett.* **53**, 1181 (1988)

[60] B. Bech Nielsen, *Phys. Rev. B* **37**, 6353 (1988)

[61] H. J. Stein, *Phys. Rev. Lett.* **43**, 1030 (1979)

[62] A. Van Wieringen and N. Warmoltz, *Physica* **22**, 849 (1956)

[63] C. H. Seager, R. A. Anderson, J. K. G. Panitz, *J. Mater. Res.* **2**, 96 (1987)

[64] T. Ichimiya, A. Furuichi, *Int. J. Appl. Rad. Isotopes* **19**, 573 (1968)

[65] T. S. Shi, S. N. Sahu, G. S. Oehrlein, and J. W. Corbett, *Phys. Status Solidi A* **74**, 329 (1982)

[66] B. N. Mukashev *et al.*, *Phys. Lett.* **87A**, 376 (1982)

[67] S. T. Picraux and F. L. Vook, *Phys. Rev. B* **18**, 2066 (1978)

[68] B. Bech Nielsen, in *Oxygen, Carbon, Hydrogen and Nitrogen in Crystalline silicon*, edited by J. C. Mikkelsen *et al.*, MRS Symposia Proceedings No. 59 (Materials Research Society, Pittsburgh, PA, 1986), p. 487

[69] R. F. Kiefl, M. Celio, T. L. Estle, S. R. Kreitzman, G. M. Luke, T. M. Riseman and E. J. Ansaldo, *Phys. Rev. Lett.* **60**, 224 (1988)

[70] M. Capizzi and A. Mittiga, *Physica* **146B**, 19 (1987)

[71] A. E. Jaworowski, *Radiation Effects and Defects in Solids* , to be published

[72] A. Mainwood, and A. M. Stoneham, *J. Phys. C* **17**, 2513 (1984)

[73] M. J. Gillan, *Phys. Rev. Lett.* **58**, 563 (1987)

[74] H. R. Schober, and A. M. Stoneham, *Phys. Rev. Lett.* **60**, 2307 (1988)

[75] A. M. Stoneham, *Faraday Trans. I J. Chem. Soc.* , to be published

[76] G. G. DeLeo, and W. B. Fowler, *Phys. Rev. B* **31**, 6861 (1985)

[77] A. Amore Bonapasta, A. Lapicciarella, N. Tomassini, and M. Capizzi, *Phys. Rev. B* **36**, 6228 (1987)

[78] K. J. Chang, and D. J. Chadi, *Phys. Rev. Lett.* **60**, 1422 (1988)

[79] P. J. H. Denteneer, C. G. Van de Walle, and S. T. Pantelides, *Phys. Rev. B* **39**, 10809 (1989)

[80] S. Estreicher, *Phys. Rev. B* **37**, 858 (1988)

[81] A. Amore Bonapasta, A. Lapicciarella, N. Tomassini, and M. Capizzi, *Europhys. Lett.* **7**, 145 (1988)

[82] C. G. Van de Walle, Y. Bar-Yam and S. T. Pantelides, *Phys. Rev. Lett.* **60**, 2761 (1988)

[83] P. Deak, L. C. Snyder, and J. W. Corbett, *Phys. Rev. B* **37**, 6887 (1988)

[84] S. Estreicher, *Phys. Rev. B* **36**, 9122 (1987)

[85] C. G. Van de Walle, P. J. H. Denteneer, Y. Bar-Yam and S. T. Pantelides, *Phys. Rev. B* **39**, 10791 (1989)

[86] C. Pennetta, *Solid State Commun.* **69**, 305 (1989)

[87] F. Buda, G. L. Chiarotti, R. Car and M. Parrinello, *Phys. Rev. Lett.* **63**, 294 (1989)

[88] A. J. Tavendale, D. Alexiev and A. A. Williams, *Appl. Phys. Lett.* **47**, 316 (1985)

[89] T. Zundel, E. Courcelle, A. Mesli, J. C. Muller and P. Siffert, *Appl. Phys. A* **40**, 67 (1986)

[90] W. Weber, *Phys. Rev. B* **15**, 4789 (1977)

[91] G. Lucovsky, R. J. Nemanich, J. C. Knights, *Phys. Rev. B* **19**, 2064 (1979)

[92] M. H. Brodshy, M. Cardona, J. J. Cuomo, *Phys. Rev. B* **16**, 3556 (1977)

[93] W. E.Spear and P. G. LeComber, *Solid State Commun.* **17**, 1193 (1975)

[94] W. E.Spear and P. G. LeComber, *Phil. Mag.* **33**, 935 (1976)

[95] W. E.Spear, P. G. LeComber, S. Kinmond and M. H. Brodsky, *Appl. Phys. Lett.* **28**, 105 (1976)

[96] S. R. Elliott, *Advances in Physics* **38**, 1 (1989)

[97] R. Bellisent, A. Chenevas-Paul, P. Chieux and A. Menelle, *J. Non-Crystalline Solids* **77-78**, 213 (1985)

[98] R. Bellisent, A. Menelle, A. Chenevas-Paul, and P. Chieux, *J. Phys. Paris* **46**, C8-93 (1985)

[99] A. Menelle, Ph.D. thesis, Paris (1987)

[100] D. Wang, Y. Li, H. Wei C. Tang, H. Yan, and S. Huang, *J. Non-Crystalline Solids* **95-96**, 841 (1987)

[101] S. Mobilio and A. Filipponi, *J. Non-Crystalline Solids* **97-98**, 365 (1987)

[102] A. Menelle, A. M. Flank, P. Lagarde, and R. Bellisent, *J. Phys., Paris* **47**, C8-375 (1986)

[103] W. A. Kamitakahara, H. R. Shanks, J. F. McClelland, U. Buchenau, F. Gompf, and L. Pintchovious, *Phys. Rev. Lett.* **52**, 644 (1984)

[104] W. A. Kamitakahara, C. M. Soukoulis, H. R. Shanks, U. Buchenau, G. S. Grest, *Phys. Rev. B* **36**, 6539 (1987)

[105] see for a review, J. A. Reimer, *J. Phys. Paris* **42**, C4-715 (1981)

[106] P. A. Fedders and A. E. Carlsson, *Phys. Rev. Lett.* **58**, 1156 (1987)

[107] R. Fish and D. C. Licciardello, *Phys. Rev. Lett.* **41**, 889 (1978)

[108] Y. Hishikawa *et al.*, *J. Non-Crystalline Solids* **97-98**, 399 (1987)

[109] K. Zellama *et al.*, *Phys. Rev. B* **23**, 6648 (1981)

[110] J. Baum *et al.*, *Phys. Rev. Lett.* **56**, 1377 (1986)

[111] I. Stich, R. Car, M. Parrinello, to be published

[112] S. T. Pantelides, *Phys. Rev. Lett.* **57**, 2979 (1986)

[113] S. T. Pantelides, *Phys. Rev. Lett.* **58**, 1344 (1987)

[114] R. Biswas, G. S. Grest and C. M. Soukoulis, *Phys. Rev. B* **36**, 7437 (1987)

[115] F. Buda, G. L. Chiarotti, I. Stich, R. Car and M. Parrinello, *J. Non-Crystalline Solids* , to appear

[116] R. Biswas, C. Z. Wang, C. T. Chan, K. M. Ho and C. M. Soukoulis, *Phys. Rev. Lett.* **63**, 1491 (1989)

[117] R. Tsu, in *Disordered Semiconductors*, edited by G. A. Thomas, S. R. Ovshinsky and M. Kastner, (New York: Plenum 1987) p.479

[118] S. C. Shen, C. J. Fang, M. Cardona, and L. Genzel, *Phys. Rev. B* **22**, 2913 (1980)

[119] See for example the review of Lucovsky and Pollard *in ref. [2]*,

[120] P. J. H. Denteneer and W. van Haeringen, *J. Phys. C* **18**, 4127 (1985)

[121] J. L. Martins and M. L. Cohen, *Phys. Rev. B* **37**, 6134 (1988)